Mate discrimination among subspecies through a conserved olfactory pathway

Mohammed A. Khallaf[1], Thomas O. Auer[2], Veit Grabe[1], Ana Depetris-Chauvin[1], Byrappa Ammagarahalli[3,7], Dan-Dan Zhang[4], Sofía Lavista-Llanos[1], Filip Kaftan[5], Jerrit Weißflog[5], Luciano M. Matzkin[6], Stephanie M. Rollmann[3], Christer Löfstedt[4], Aleš Svatoš [5], Hany K.M. Dweck[1,8], Silke Sachse[1], Richard Benton[2], Bill S. Hansson[1,‡] and Markus Knaden[1,‡]

[1]Department of Evolutionary Neuroethology
Max Planck Institute for Chemical Ecology
Hans-Knöll-Straße 8
D-07745, Jena, Germany

[2]Center for Integrative Genomics
Faculty of Biology and Medicine, University of Lausanne
CH-1015, Lausanne, Switzerland

[3]Department of Biological Sciences
University of Cincinnati
OH 45221, Cincinnati, USA

[4]Department of Biology
Lund University
SE-22362, Lund, Sweden

[5]Group of Mass Spectrometry and Proteomics
Max Planck Institute for Chemical Ecology
Hans-Knöll-Straße 8
D-07745, Jena, Germany

[6]Department of Entomology
University of Arizona
1140 E. South Campus Drive, Tucson, AZ 85721, USA

[7]Present address: Faculty of Forestry and Wood Sciences
Czech University of Life Sciences
165 00 Prague, Czech Republic.

[8]Present address: Department of Molecular,
Cellular, and Developmental Biology, Yale University
CT 06520, New Haven, USA

[‡]Correspondence: mknaden@ice.mpg.de (M.K.)
hansson@ice.mpg.de (B.S.H)

Abstract

Communication mechanisms underlying the sexual isolation of species are poorly understood. Using four subspecies of *Drosophila mojavensis* as a model, we identify two novel behaviorally-active, male-specific pheromones. One functions as a conserved male anti-aphrodisiac in all subspecies and acts via gustation. The second induces female receptivity via olfaction exclusively in the two subspecies that produce it. Genetic analysis of the cognate receptor for the olfactory pheromone indicates an important role for this sensory pathway in promoting sexual isolation of subspecies, in combination with auditory signals. Surprisingly, the peripheral sensory pathway detecting this pheromone is conserved molecularly, physiologically and anatomically across subspecies. These observations imply that subspecies-specific behaviors arise from differential interpretation of the same peripheral cue, reminiscent of sexually-conserved detection but dimorphic interpretation of male pheromones in *D. melanogaster*. Our results reveal that, during incipient speciation, pheromone production, detection and interpretation do not necessarily evolve in a coordinated manner.

Introduction

One of the central questions in evolutionary biology is how populations within a species split to form new species. Divergence in sexual communication – male traits and female preferences (*1*) – has been proposed as one of the significant forces that results in reproductive isolation. This divergence is more pronounced in allopatric populations as a by-product of ecological adaptation to different environments (*2*). However, despite numerous documented interspecific sexual traits and preferences in animals, the genetic and neural correlates of their evolution remain elusive (*3*).

Sexual traits of drosophilid flies differ quantitatively and qualitatively between species and act as pre-mating isolation barriers (*4*). Such traits therefore represent attractive models to determine the genetic basis of phenotypic evolution. Flies identify con-subspecific mating partners through integration of different sensory modalities such as vision, audition, olfaction, and gustation, which promote courtship of appropriate mates and inhibit courtship of inappropriate partners. Insights have been gained regarding the evolution of different sensory modalities that relate to the interspecific variations in male traits or female perception among drosophilids (e.g., vision (*5*), audition (*6*), and taste (*7, 8*)). However, even though many studies have reported the diversity of volatile pheromones in drosophilid males (*9*), the evolution of the corresponding neural changes remains little studied.

In *D. melanogaster*, sex pheromones are detected by chemosensory receptors (e.g., odorant receptors (ORs)) (*10*) expressed in sensory neurons housed in hair-like structures called sensilla. Volatile pheromone-responsive ORs represent an ideal set of candidate genes to address the evolutionary basis of various sexual traits in drosophilid flies for several reasons. First, pheromone ORs are expected to be the fastest evolving chemosensory receptors, with new receptors emerging either by

sequence variation or gene loss/duplication (*11*), to match the dramatic diversity of pheromones among closely related species (*9*). Second, the neural processing of some drosophilid pheromones (e.g., (*Z*)-11-octadecenyl acetate (*cis* vaccenyl acetate, *c*VA) in *D. melanogaster*) in the brain is well understood (*10*). Third, pheromone ORs are narrowly tuned to fly odors and govern robust and distinct behaviors via labeled-line circuitry (*12-15*). Fourth, olfactory sensory neurons (OSNs) that express pheromone ORs target sexually-dimorphic pheromone-processing units (i.e., antennal lobe glomeruli) (*12*). Finally, out of 52 OSN classes in *D. melanogaster* (*16*), only four pheromone OR-expressing OSNs are localized in a one class of sensillum (Or67d neuron in antennal trichoid 1 (at1) and Or47b, Or65a/b/c and Or88a neurons in at4) (*17*). This small number compared to other non-pheromone-detecting OSNs (*17*) makes a comprehensive evolutionary study feasible.

One remarkable drosophilid is *D. mojavensis*, which represents a model of incipient speciation and host adaptation (*18*). This species has four geographically-isolated and ecologically-distinct populations (*19*) (taxonomically classified as subspecies (*20*)) that diverged ~0.25 million years ago (*18, 19*) (Fig. 1A). The northern subspecies *D. moj. wrigleyi* and *D. moj. mojavensis* use prickly pear cacti in Santa Catalina Island and red barrel cactus in the Mojave Desert, respectively, as host fruit. The southern subspecies *D. moj. sonorensis* and *D. moj. baja* breed and feed on the organ pipe cactus in the mainland Sonoran Desert and the agria cactus in Baja California, respectively (*21*). Phylogenetic analyses revealed that the two northern subspecies and the two southern subspecies cluster with each other (Fig. 1B and fig. S1A) (*22*). These closely-related subspecies exhibit many differences in their morphology (*20*), neurophysiological responses (*23*), genomic and transcriptomic characteristics (*18, 22*), and behavioral traits (*24*). Experimental reciprocal crosses between these allopatric subspecies resulted in viable fertile offspring, indicating the presence of prezygotic isolation mechanisms (*25, 26*). Previous evidence suggested that cuticular hydrocarbons contribute to this isolation barrier (*27*), but no specific chemicals have been isolated. Here we identify these pheromones and elucidate the evolution of the underlying sensory mechanisms across subspecies to reveal the neurogenetic basis of incipient speciation.

Results

Sexual isolation among incipient subspecies of *D. mojavensis*

We compared the courtship ritual among the four subspecies of *D. mojavensis* by recording the sexual behaviors of con-subspecific couples in a single-pair courtship arena (movies S1 to S4). *D. mojavensis* subspecies displayed comparable courtship rituals including a trait not described in other drosophilids – dropping behavior – in which males release a liquid droplet from their anus while licking the female's genitalia (fig. S1, B to H).

We asked whether *D. mojavensis* flies can distinguish con-subspecific and hetero-subspecific partners. As copulation success is influenced by both male

133 courtship intensity and female receptivity (*4*), we first examined whether males exhibit
134 courtship preference towards con-subspecific females. To distinguish male sexual
135 behaviors from female acceptance, males were offered the choice to court either a
136 freeze-killed con-subspecific or hetero-subspecific female (fig. S1I). Males exhibited
137 equal preferences between females, regardless of their subspecies (fig. S1I).
138 Next, we investigated whether females of the different subspecies are able to
139 distinguish their con-subspecific males by offering a female of each subspecies the
140 choice to mate with a con-subspecific male or a male of one of the other three
141 subspecies (Fig. 1C). Competition experiments with the two northern subspecies
142 revealed that females did not distinguish con-subspecific and hetero-subspecific males
143 (Fig. 1C). By contrast, southern females strongly preferred to copulate with their con-
144 subspecific males (Fig. 1C). Both northern and southern females efficiently
145 discriminated northern and southern males (Fig. 1C). These results suggest that while
146 a complete sexual isolation barrier has been established both between the northern
147 and southern subspecies, and between the southern subspecies, the northern
148 subspecies are not yet completely sexually isolated.
149
150 ***D. mojavensis* subspecies have distinct, but overlapping, profiles of candidate**
151 **pheromones**
152
153 To identify candidate pheromones that could mediate the observed sexual isolation
154 barriers between subspecies, we analyzed the chemical profiles of males, virgin
155 females and mated females of several independent isolates of each subspecies. We
156 discovered four previously unknown male-specific acetates (Fig. 2, A and B and fig.
157 S2A) as (*R*) and (*S*) enantiomers of (*Z*)-10-heptadecen-2-yl acetate (R&S-HDEA),
158 heptadec-2-yl acetate (HDA) and (*Z,Z*)-19,22-octacosadien-1-yl acetate (OCDA).
159 Males of all four subspecies carried OCDA, while only males of the northern
160 subspecies produced HDEA (both *R* and *S* enantiomers in similar ratio (fig. S2, B and
161 C)) and HDA (Fig. 2, A and B and fig. S2, A and A'). The chemical profiles of the virgin
162 females were similar among the different subspecies (Fig. 2A and fig. S2A), which
163 might explain the males' inability to distinguish between them (fig. S1I). However,
164 mated females carried male-specific compound(s), indicating that these are
165 transferred from males to females during mating (Fig. 2, A and B and fig. S2A). Using
166 matrix-assisted laser desorption/ionization-time of flight (MALDI-TOF) analyses to
167 directly visualize pheromones on the fly body (see Materials and Methods for details),
168 we confirmed the existence of OCDA on the male and mated female cuticle, but not
169 on the virgin females (fig. S2, D and E).
170 We next investigated whether production of the male-specific compounds
171 correlates with male sexual maturity and copulation performance. Males of the four
172 subspecies did not exhibit any copulation during the first five days post-eclosion (i.e.,
173 in absence of the acetates), showed low copulation success rates at the age of six
174 days (when low amounts of acetates were already detected), and successfully mated
175 from the seventh day on (Fig. 2C). These observations suggest that the identified male-
176 specific acetates define the sexual maturity status of males.

The ubiquitous pheromone, OCDA, acts as conserved male anti-aphrodisiac via contact chemosensation

We asked if transfer of any male-specific compounds contributes to a general post-copulation mate-guarding strategy in *D. mojavensis* (as described for transferred pheromones in *D. melanogaster* (*28, 29*)). The identical chemical profiles of the two northern subspecies, and of the two southern subspecies led us to focus our attention on one representative for each group. Males of *D. moj. wrigleyi* and *D. moj. sonorensis* spent more time courting virgin than mated con-subspecific females (Fig. 3A). To test which, if any, of the identified compounds contribute to courtship reduction, we perfumed virgin con-subspecific females with one of the four male-specific compounds (consistency of perfuming and correspondence to biologically relevant amounts were confirmed by GC-MS analysis; see Materials and Methods). Only OCDA treatment of females led to a significantly reduced male courtship index (Fig. 3B and fig. S3A).

To investigate how males detect OCDA, we first tested the volatility of male-specific acetates (including OCDA) by collecting headspace samples of *D. moj. wrigleyi* males (fig. S3B). This revealed that only R&S-HDEA and HDA are volatile (fig. S3B) indicating that the non-volatile OCDA is likely to be detected by gustation. During courtship, neural inputs from foreleg gustatory sensilla are used to evaluate the potential mating partner (*4*). We therefore investigated whether male foreleg tarsi detect OCDA (Fig. 3C). Indeed, OCDA, but not the other acetates, elicited a response in a subset of tarsal sensilla (class 5b) of both *D. mojavensis* subspecies (Fig. 3C and fig. S3, C and D). Consistent with these sensilla mediating detection of OCDA, males lacking their tarsi spend equal time courting the hexane-perfumed and OCDA-perfumed females (Fig. 3D). We propose that OCDA has a conserved role across the *D. mojavensis* subspecies as a contact chemosensory signal that suppresses male courtship of mated females.

R-HDEA promotes subspecies-specific female sexual receptivity through olfaction

To examine the functions of the other novel male-specific acetates in female sexual behaviors, we scored the copulation success and latency for *D. moj. wrigleyi* and *D. moj. sonorensis* females courted by con-subspecific males. Males were perfumed with one of the four male-specific acetates or hexane. Copulation success and courtship indices did not differ between the acetate- and hexane-perfumed males in both subspecies (Fig. 4A and figs. S3E and S4A). However, females of *D. moj. wrigleyi* were significantly quicker to accept the R-HDEA-perfumed males but not the males perfumed with the other acetates (Fig. 4B and fig. S4B). We extended this analysis by performing competition assays, in which a virgin female of each subspecies was allowed to choose between two con-subspecific males perfumed with hexane or with one of the four acetates. Only R-HDEA-perfumed males exhibited copulation advantage over the controls in *D. moj. wrigleyi* and *D. moj. mojavensis*, while *D. moj. sonorensis* and *D. moj. baja* females had comparable preferences between the two

222 males (Fig. 4C and fig. S4, C and D). These results indicate that R-HDEA increases
223 sexual receptivity in females of northern but not southern subspecies.

224 As R-HDEA is volatile (fig. S3B), we screened for olfactory sensory neurons
225 (OSNs) that detect R-HDEA in *D. moj. wrigleyi* via single sensillum recordings (SSR).
226 We identified a single antennal trichoid sensillum class, at4 (based upon presumed
227 homology to the *D. melanogaster* at4 sensillum; see below) that responds strongly to
228 R-HDEA and HDA (Fig. 4, D and E and fig. S4, E to G). Our extensive screening of *D.*
229 *moj. sonorensis* OSNs, as well as limited recordings in *D. moj. mojavensis* and *D. moj.*
230 *baja*, revealed a presence of a sensillum with identical response properties in all four
231 subspecies (Fig. 4, E and F and fig. S4, E and H). Taken together, R-HDEA activates
232 homologous olfactory channels in all subspecies of *D. mojavensis* and enhances
233 sexual receptivity in *D. moj. wrigleyi* but not in *D. moj. sonorensis* females.
234

235 **Conserved peripheral sensory pathways for R-HDEA detection**

236

237 To define the genetic basis of R-HDEA detection in *D. mojavensis* subspecies, we
238 focused on a subset of receptors, which was previously shown to be expressed in
239 trichoid OSNs and to detect pheromones in *D. melanogaster* (*12, 13, 17, 30*). Five
240 orthologous genes are present in the *D. moj. wrigleyi* genome (*11*): *Or47b1*, *Or47b2*,
241 *Or65a*, *Or67d* and *Or88a* (fig. S5A). We first visualized their expression in the antenna
242 of *D. moj. wrigleyi* and *D. moj. sonorensis* by RNA *in situ* hybridization and detected
243 expression of all receptors with a slightly increased number of *Or65a* and *Or67d*-
244 expressing cells in *D. moj. wrigleyi* (Fig. 5, A and B). We then asked which of these
245 ORs is responsible for R-HDEA detection by functional expression in *Xenopus laevis*
246 oocytes (Fig. 5C). We could detect significant depolarization upon R-HDEA application
247 for OR47b1 and OR65a (Fig. 5D and fig. S5B). To validate these results, we generated
248 transgenic flies expressing *D. moj. wrigleyi* ORs individually *in vivo* in the at1 "decoder"
249 neuron of *D. melanogaster* that lacks its endogenous receptor OR67d (*12*) (Fig. 5E).
250 SSR analysis of these flies revealed that OR65a, but not OR47b1, is the sole detector
251 for R-HDEA and HDA (Fig. 5F and fig. S5C). As predicted by the similar responses of
252 at4 sensilla to R-HDEA and OR65a sequence similarity between both subspecies (Fig.
253 4, E and G and fig. S5G), transgenic expression of *D. moj. sonorensis* OR65a in the
254 decoder neuron revealed comparable responses to R-HDEA (Fig. 5G).

255 To determine whether *Or65a* is required for the enhanced female receptivity in
256 *D. moj. wrigleyi*, we generated a loss-of-function allele of this gene using
257 CRISPR/Cas9 genome editing (Fig. 5H and fig. S5, E and F). *Or65a* mutant females
258 completely lack responses to R-HDEA (Fig. 5I), display no preference for R-HDEA-
259 perfumed males (Fig. 5J and fig. S5D), and take longer to initiate copulation (Fig. 5J').
260 These findings confirm that OR65a is responsible for the increased female receptivity
261 in *D. moj. wrigleyi* towards con-subspecific males.

262 We next analyzed the targeting pattern of Or65a OSNs to glomeruli in the
263 antennal lobe. Comparative morphological analyses revealed a high similarity in the
264 basic architecture of this olfactory center in *D. moj. wrigleyi* and *D. moj. sonorensis*
265 (Fig. 5K and movies S5 and 6), but with apparently at least three additional glomeruli

266 compared to the well-characterized antennal lobe of *D. melanogaster* (fig. S6A).
267 Previous genetic tracing of at4 OSNs in *D. melanogaster* revealed projections to three
268 glomeruli: Or47b neurons to VA1v, Or88a neurons to VA1d and Or65a/b/c neurons to
269 DL3 (*17*). To label these neurons in *D. mojavensis* subspecies, in absence of binary
270 effector systems, we backfilled at4 sensillum neurons with a fluorescent dye. In both
271 *D. moj. wrigleyi* and *D. moj. sonorensis*, we detected projections to three glomeruli:
272 VA1v, VA1d and a glomerulus not present in *D. melanogaster* that we named "VA8"
273 (Fig. 5L and fig. S6B and movies S7 and 8, for terminology see Materials and
274 Methods). Given the conserved innervation patterns of OSNs in the *melanogaster*
275 clade (*8, 31, 32*), it is likely that VA1v and VA1d are innervated by Or47b and Or88a
276 neurons in *D. mojavensis*, as in *D. melanogaster*. If this assumption is correct, our
277 observations imply that Or65a neurons target the VA8 glomerulus in *D. mojavensis* –
278 contrasting with the DL3 innervation pattern in *D. melanogaster* – although future
279 development of genetic reporters in *D. mojavensis* will be necessary to confirm this
280 proposition.

281 Pheromone-responsive glomeruli often display sex-specific volume differences
282 (*33*). Volumetric analysis of the glomeruli innervated by at4 neurons in both subspecies
283 revealed that *D. moj. wrigleyi* VA8 is the only sexually dimorphic unit, being 1.6-fold
284 larger in females (Fig. 5M and fig. S6, G and H). In addition, there was a non-significant
285 trend of larger volume of VA8 in *D. moj. sonorensis* females compared to males (Fig.
286 5M and fig. S6, G and H). Together, these results indicate that OR65a-expressing
287 neurons in both subspecies detect R-HDEA and exhibit similar innervation pattern in
288 the antennal lobe.
289

290 **Subspecies-specific contributions of R-HDEA and auditory cues in sexual**
291 **isolation**
292

293 As *D. moj. wrigleyi* females can distinguish between their con-subspecific males and
294 *D. moj. sonorensis* males (which lack R-HDEA (Fig. 2, A and B), Figs. 1C and 6A), we
295 asked whether R-HDEA mediates this discrimination. We presented to a *D. moj.*
296 *wrigleyi* female a choice of a *D. moj. wrigleyi* male perfumed with hexane and a male
297 of *D. moj. sonorensis* perfumed with R-HDEA. Female preference for its con-
298 subspecific male was greatly reduced (Fig. 6A' and fig. S7A). Furthermore, when given
299 a choice between two males of *D. moj. sonorensis,* of which only one was perfumed
300 with R-HDEA, *D. moj. wrigleyi* females exhibited a strong preference for the perfumed
301 ones (Fig. 6A'').

302 Despite this instructive role of R-HDEA in mate discrimination, we observed that
303 *D. moj. wrigleyi-Or65a* mutant females (which cannot detect R-HDEA) still display
304 strong preference for con-subspecific males (Fig. 6B), indicating that other cues must
305 exist. Previous reports revealed that subspecies-specific songs during courtship
306 induce mate recognition among *D. mojavensis* subspecies (*34*). We therefore
307 investigated whether auditory inputs are sufficient to mediate mate recognition.
308 Aristaless *D. moj. wrigleyi* females – lacking an essential part of the antennal auditory
309 organ – still exhibited normal preference for aristaless con-subspecific males over

aristaless hetero-subspecific ones (Fig. 6B'). However, aristaless, *Or65a* mutant females exhibited a major loss in the recognition of con-subspecific males (Fig. 6B''). These results indicate that R-HDEA and auditory cues have redundant roles in permitting subspecies discrimination of *D. moj. wrigleyi*.

In contrast to *D. moj. wrigleyi* females, *D. moj. sonorensis* females preferred con-subspecific males over the *D. moj. wrigleyi* one, even when the con-subspecific one was perfumed with R-HDEA or other male-specific compounds (Fig. 6C and fig. S7B). This subspecies appears to rely solely on auditory input for subspecies recognition, as aristaless females displayed indiscriminate preference for con-subspecific and hetero-subspecific males (Fig. 6C').

Discussion

Modifications in sex pheromones and their cognate sensory detection mechanisms are thought to provide a rapid means to alter mate recognition abilities during the evolution of new species (*3*). Our results provide several novel insights into how intra- (between *D. mojavensis* subspecies) and interspecific (between species across *Drosophila* genus) sexual barriers arise.

First, among *D. mojavensis* subspecies, we identified four male-specific acetates of which three were exclusively produced by the northern subspecies (Fig. 2, A and B). This dramatic change in chemical profile is surprising given the relatively short divergence time of ~0.25 million years between *D. mojavensis* subspecies (*18, 19*). Although these subspecies utilize different host cacti in nature (*18*), they were bred on the same food in our study, suggesting that the different chemical profiles are not a consequence of nutrition but rather genetically determined. The male-specificity and copulation-dependent transfer of these acetates resembles *c*VA in *D. melanogaster*, which is produced by the ejaculatory bulb and transferred to females during mating. Our data reveal, however, that the sex-specific *c*VA-induced behaviors in *D. melanogaster* (*12, 28*) – inhibiting male and inducing female mating behaviors – are mediated by different compounds in *D. mojavensis*. OCDA is present and suppresses male courtship in both *D. mojavensis* subspecies, while R-HDEA induces female receptivity in the subspecies that produce it. Consistent with OCDA-induced behaviors, a recent study (*35*) showed that *D. mojavensis* males avoid courting females perfumed with ejaculatory-bulb extracts of mature males.

Second, our results address a longstanding mystery of the modalities that determine prezygotic isolation between *D. mojavensis* subspecies (*25, 26*). *D. mojavensis* subspecies display identical courtship elements, indicating that the sexual isolation (Fig. 1C) is due to different subspecies- specific traits and preferences. We provide evidence that the dedicated R-HDEA-sensing neurons and auditory cues collaborate to mediate mate recognition in *D. moj. wrigleyi*. By contrast, R-HDEA did not induce any behavioral change in *D. moj. sonorensis* females that rely only on auditory cues (i.e., the subspecies-specific song (*34*)) for mate recognition. The striking change of R-HDEA-induced behaviors (Fig. 4C and fig. S4D) – despite its conserved peripheral sensory pathway (Figs. 5E and 6B-C) – implies the existence of differences

354 in the central processing pathways among *D. mojavensis* subspecies. These findings
355 are reminiscent of sexually-dimorphic behavioral responses to *c*VA in *D. melanogaster*
356 (*36*), which are thought to arise from sex-specific central neuronal connectivity patterns
357 downstream of non-dimorphic sensory neuron populations (*37*).

358 Third, although males of *D. melanogaster* and some Hawaiian *Drosophila*
359 species have been shown to attract females over distance by releasing pheromones
360 in fecal droplets (*38, 39*), the release of droplets during close courtship has not, to our
361 knowledge, been described in other drosophilid species. In *D. moj. wrigleyi*, this droplet
362 contains the volatile sex pheromone R-HDEA (fig. S2G), which increases female
363 receptivity. Such a trait might be related to the sexual behavior of *D. mojavensis*
364 observed in nature, where males attract females to undamaged areas next to the
365 necrotic feeding sites on cacti (*38*).

366 Fourth, the presence of different male-specific compounds in *D. mojavensis*
367 compared to other drosophilids (*9*)) raises the possibility of a rapid divergence in the
368 tuning of the corresponding sensory receptors (*23, 31*). We demonstrate that the
369 diverged OR65a orthologs of *D. mojavensis* and *D. melanogaster* (fig. S4J) have
370 different functional properties; the *D. melanogaster*-Or65a is not detecting the best
371 ligand of *D. moj. wrigleyi*-OR65a, R-HDEA, and *vice versa* (Fig. 4E and fig. S4I and
372 fig. S5C). In-line with the functional divergence, the number of Or65 gene copies is
373 frequently changing along the *Drosophila* phylogeny (*11*), indicating that the variation
374 at this locus could be important for the evolution of novel olfactory channels (*11*).

375 Finally, divergence of the chemosensory genes among closely-related
376 *Drosophila* species could be accompanied by a physiological alteration in the
377 underlying central circuitry (*8*). Our results provide, to our knowledge, the first
378 correlation between anatomical difference and divergent behaviors of homologous
379 neurons. The likely conserved innervation pattern of neurons expressing *Or47b* and
380 *Or88a* implies that Or65a neurons in *D. melanogaster* and *D. mojavensis* have evolved
381 novel projection patterns in the antennal lobe, targeting DL3 in *D. melanogaster* and
382 VA8 in *D. mojavensis*. The intriguing wiring of the Or65a in *D. mojavensis* indicates
383 that it could be partnering with another subset of second-order neurons responsible for
384 the different type of sexual behaviors: Or65a mediates female receptivity in *D. moj.*
385 *wrigleyi*, whereas it inhibits female attraction toward *c*VA in *D. melanogaster* (*40*).
386 However, more advanced genetic tools will be necessary to confirm this anatomical
387 difference and to functionally characterize the olfactory pathways of the *D. mojavensis*
388 subspecies.

389 Future evolutionary investigations of the innervation pattern of R-HDEA-
390 responsive neurons in the higher brain centers will shed light on the divergent functions
391 of R-HDEA among the closely related subspecies of *D. mojavensis* and will explain
392 how neural circuits coevolve with sex pheromones to permit specific mate recognition.

393
394
395
396
397

398 **Materials and Methods**
399
400 ***Drosophila* lines and chemicals**
401 **Fly stocks.** Wild-type flies used in this study were obtained from the National
402 *Drosophila* Species Stock Centre (NDSSC) (https://stockcenter.ucsd.edu). Stock
403 numbers and breeding diets are listed in table S1. Transgenic *D. melanogaster* flies
404 and *D. mojavensis* knock-out lines generated in this study are listed in table S1. All
405 flies were reared at 25°C, 12 h Light:12 h Dark and 50% relative humidity. For more
406 details on the food recipes see *Drosophila* Species Stock Centre
407 (http://blogs.cornell.edu/drosophila/recipes/) or (*41*). Animals subjected to arista or
408 foreleg removal were left to recover for 2 days post-surgery before behavioral
409 experiments.
410 **Chemicals.** Odorants used in this study, sources, and CAS numbers are listed in the
411 table S1. All odors were diluted in dichloromethane (DCM) for SSR, in dimethyl
412 sulfoxide (DMSO) for oocytes and tip recording experiments or in hexane for
413 behavioral experiments.
414
415 **Chemical analyses**
416 **Thermal Desorption-Gas Chromatography-Mass Spectrometry (TD-GC-MS).**
417 Individual flies or ejaculatory bulbs were prepared or dissected, respectively, for
418 chemical profile collection as described previously (*13*), with some modifications.
419 Briefly, the GC-MS device (Agilent GC 7890A fitted with an MS 5975C inert XL MSD
420 unit; www.agilent.com) was equipped with an HP5-MS UI column (19091S-433UI;
421 Agilent Technologies). After desorption at 250°C for 3 min, the volatiles were trapped
422 at -50°C using liquid nitrogen for cooling. In order to transfer the components to the
423 GC column, the vaporizer injector was heated gradually to 270°C (12°C/s) and held for
424 5 min. The temperature of the GC oven was held at 50°C for 3 min, gradually increased
425 (15°C/min) to 250°C and held for 3 min, and then to 280°C (20°C/min) and held for 30
426 min. For MS, the transfer line, source and quad were held at 260°C, 230°C and 150°C,
427 respectively. Eluted compounds for this and the following analyses were ionized in
428 electron ionization (EI) source using electron beam operating at 70 eV energy and their
429 mass spectra were recorded in positive ion mode in the range from *m/z* 33 to 500. Anal
430 droplets of courting males were collected on a cover glass (22 × 22 mm, Cat. No.: 631-
431 0126, https://uk.vwr.com) and analyzed by TD-GC-MS. The structures of the newly
432 identified acetates were confirmed by comparing their mass spectrum with synthesized
433 standards.
434 **Body extract analysis by GC-MS.** Fly body extracts were obtained by washing single
435 flies of the respective sex, age and mating status in 10 µl of hexane for 30 min. For GC
436 stimulation, 1 µl of the odor sample was injected in a DB5 column (Agilent
437 Technologies; www.agilent.com), fitted in an Agilent 6890 gas chromatograph, and
438 operated as described previously (*42*). The inlet temperature was set to 250°C. The
439 temperature of the GC oven was held at 50°C for 2 min, increased gradually (15°C/min)
440 to 250°C, which was held for 3 min, and then to 280°C (20°C/min) and held for 30 min.
441 The MS transfer-line, source and quad were held at 280°C, 230°C and 150°C,
442 respectively. Average amounts of HDEA, HDA and OCDA from individual flies were

443 quantified by comparing their peak areas with the area of hexadecane (10 ng), which
444 was added to the fly extract as an internal standard.
445 **Chiral chromatography.** To check the ratio of (2*R*,10Z)-10-Heptadecen-2-yl acetate
446 and (2*S*,10*Z*)-10-Heptadecen-2-yl acetate (R/S-HDEA), hexane body extracts of male
447 flies were injected into a CycloSil B column (112-6632, Agilent Technologies;
448 www.agilent.com) fitted in Agilent 6890 gas chromatograph and operated as follows:
449 The temperature of the GC oven was held at 40°C for 2 min and then increased
450 gradually (10°C/min) to 170°C, then to 200°C (1°C/min), and finally to 230°C
451 (15°C/min) which was held for 3 min.
452 **Matrix-assisted laser desorption/ionization-time of flight (MALDI-TOF).** MALDI-
453 TOF experiments of 13-day-old flies were performed on MALDI Micro MX (Waters, UK)
454 operated in a reflectron mode with acceleration and plate voltages at 12 and 5 kV,
455 respectively. Due to the relative high volatility and weaker ionization of R/S-HDEA and
456 HDA compared to OCDA, only OCDA signals were detected in the MSI spectra.
457 Moreover, OCDA was predominantly present in a form of $[M+K]^+$ adducts. Delayed
458 extraction time was 500 ns. Compound's desorption/ionization was realized by
459 nitrogen UV laser (337 nm, 4 ns pulse of maximum 320 µJ and frequency of 20 Hz).
460 Matrix ions were suppressed with a low mass cut-off set at *m/z* 150. Flies were fixed
461 on their dorsal side and processed as described previously (*43*). The number of laser
462 shots per spot was optimized and set to 60 (128 µJ/shot). The range of the measured
463 masses was set from *m/z* 100 to *m/z* 1000. Data were collected with MassLynx 4.0
464 software and processed with custom-made software MALDI Image Convertor (Waters,
465 UK) to obtain spatially differentiated data. These data were exported to the BioMap
466 software (Novartis, Switzerland) and converted to 2-D ion intensity heat maps. All
467 samples were analyzed in positive ion mode and imaged using a step size of 100 µm.
468 Methanolic solution of LiDHB and LiVA (in case of copulated flies) matrix in a
469 concentration of 20 mg/mL was sprayed on the fly samples by an airbrush. For one
470 sample, 0.4 mL of LiDHB/LiVA matrix solution was used to form approximately 25
471 layers. Waiting time between two consecutive sprays was 3s. Lithium 2,5-
472 dihydroxybenzoate (LiDHB) and lithium vanillate (LiVA) matrix were synthesized as
473 described previously (*44*). Polyethylene glycol oligomers (with an average molecular
474 weight of 200, 300, 600 and 1000 Da) for calibration of the mass spectrometer were
475 purchased from Sigma-Aldrich as well as precursors of the LiDHB and LiVA.
476 Potassiated adducts of OCDA at *m/z* 487 evinced a negative mass shift which was
477 observed within a range from *m/z* 0.05 to *m/z* 0.3 between measurements.
478 **Fly odor analysis by Solid Phase Microextraction (SPME).** Volatiles were collected
479 from 20 *D. moj. wrigleyi* males trapped in a mesh inside a capped 4 mL glass vials with
480 polytetrafluoroethylene-lined silicone septa (Sigma, 23242-U) to preclude flies contact
481 to the SPME fiber (grey hub plain; coated with 50/30 µm divinylbenzene/carboxen on
482 polydimethylsiloxane on a StableFlex fiber, Sigma, 57328-U). SPME fiber was
483 exposed to the trapped flies for 1 h at room temperature. The SPME fiber was then
484 retracted and immediately inserted into GC-MS system (Agilent 7890B fitted with MS
485 5977A unit) as operated previously (*45*). The inlet temperature was set to 250°C. The
486 temperature of the GC oven was held at 40°C for 3 min and then increased gradually
487 (5°C/min) to 280°C, which was held for 10 min.

488 **Perfuming flies with hexane or male-specific compounds.** Male and female flies
489 were perfumed with the acetates singly diluted in hexane or hexane alone as
490 previously described (*13*). Briefly, 10 µL of a 50 ng/µL stock solution was pipetted into
491 a 1.5-mL glass vial. After evaporating the hexane under nitrogen gas flow, ten flies
492 were transferred to the vial and subjected to three medium vortex pulses lasting for 30
493 s, with a 30-s pause between each pulse. Flies were transferred to fresh food to
494 recover for 2 h and then introduced to the courtship arenas or subjected to GC-MS
495 analysis to confirm the increased amount of the perfumed acetate. Each fly was coated
496 with ~1-3 ng of the compound of interest. This amount is comparable to that naturally
497 present on male flies (Fig. 2C).
498
499 **Chemical identification and synthesis**
500 (provided as a separate word file)
501
502 **Behavioral experiments**
503 **Single and competitive mating assays.** Males and females were collected after
504 eclosion and raised individually and in groups, respectively. For each experiment,
505 courtship assays were performed in a chamber (1 cm diameter × 0.5 cm depth)
506 covered with a plastic slide. Courtship behaviors were recorded for 10 or 20 min using
507 a GoPro Camera 4 or Logitech C615 as stated in the figure legends. All single mating
508 experiments were performed under red light (660 nm wavelength) at 25°C and 70%
509 humidity. Each video was analyzed manually for copulation success, which was
510 measured by the percentage of males that copulated successfully in the first 10 min,
511 copulation latency, which was measured as the time taken by each male until the onset
512 of copulation, and courtship index, which was calculated as the percentage of time that
513 the male spends courting the female during 10 min. In all competition experiments,
514 copulation success was manually monitored for 1 h. Freeze-killed females were used
515 in the courtship assays to disentangle male sexual behaviors from female acceptance.
516 Freshly-mated females have been mated for the first time and were used in the
517 experiments of Fig. 3 to ensure that the compounds transferred to females were still
518 present.
519 In the competition mating assays, rival flies were marked by UV-fluorescent
520 powder of different colors (red: UVXPBR; yellow: UVXPBB; green: UVXPBY;
521 purchased from Maxmax.com; https://maxmax.com/) 24 h before the experiments.
522 Competition assays were manually observed for 1 h and copulation success was
523 scored identifying the successful rival under UV light. Females killed by freezing were
524 used to calculate the courtship index of males in presence of the different acetates and
525 hexane perfumed females or con-specific and hetero-subspecific females. Data from
526 competition experiments represents either females courted by both rival males or
527 males courted with both rival females to ensure that females or males chose between
528 rival pairs and did not simply copulate or court with the first partner they encountered.
529 Results from females that were only courted by one male, or males that only courted
530 one female were excluded. For tarsi- or arista-less flies either the first three segments
531 of male tarsi or both aristae were clipped with a clean razor blade and flies were kept
532 to recover for 2 days on fresh food before introduction into the courtship arena. All

533 courtship and copulation data were acquired by a researcher blinded to the treatment.
534 For collecting male anal droplets, a virgin male and a decapitated female were kept in
535 a courtship chamber covered with a glass coverslip. Males were allowed to court and
536 discharge the anal droplets on the glass coverslips which were then cracked to small
537 pieces and inserted into the TD-GC-MS tubes for analysis. As a control, glass
538 coverslips were sampled from courtship arenas containing only males.
539
540 **Electrophysiological and molecular biology experiments**
541 **Single sensillum recording (SSR).** Adult flies were immobilized in pipette tips, and
542 the third antennal segment was placed in a stable position onto a glass coverslip (*46*).
543 Sensilla types were localized under a microscope (BX51WI; Olympus) at 100×
544 magnification and identified by diagnostic odors stated in table S1. The extracellular
545 signals originating from the OSNs were measured by inserting a tungsten wire
546 electrode in the base of a sensillum and a reference electrode into the eye. Signals
547 were amplified (Syntech Universal AC/DC Probe; Syntech), sampled (10,667.0
548 samples/s), and filtered (300 – 3,000 Hz with 50/60 Hz suppression) via USB-IDAC
549 connection to a computer (Syntech). Action potentials were extracted using AutoSpike
550 software, version 3.7 (Syntech). Synthetic compounds were diluted in
551 dichloromethane, DCM, (Sigma-Aldrich, Steinheim, Germany). Prior to each
552 experiment, 10 µl of diluted odor was freshly loaded onto a small piece of filter paper
553 (1 cm^2, Whatman, Dassel, Germany), and placed inside a glass Pasteur pipette. The
554 odorant was delivered by placing the tip of the pipette 2 cm away from the antennae.
555 Neuron activities were recorded for 10 s, starting 2 s before a stimulation period of 0.5
556 s. Responses from individual neurons were calculated as the increase (or decrease)
557 in the action potential frequency (spikes/s) relative to the pre-stimulus frequency.
558 Traces were processed by sorting spike amplitudes in AutoSpike, analysis in Excel
559 and illustration in Adobe Illustrator CS (Adobe systems, San Jose, CA).
560 **Tip recording.** Tip recordings from tarsal sensilla were performed as described
561 previously (*47*). Male flies (8-10 day old) were immobilized in pipette tips, and the
562 foreleg was fixed with Scotch tape onto a glass coverslip. A reference glass electrode
563 filled with Ringer's solution (140 mM NaCl, 3 mM $MgCl_2$, 2 mM $CaCl_2$, 10 mM D-
564 glucose, 10 mM HEPES, pH 7.4) was inserted into the thorax of the fly. The different
565 tarsal sensilla were stimulated by placing a glass capillary filled with OCDA (10 µg)
566 dissolved in DMSO on the sensillum tip. The recording electrode was connected to a
567 pre-amplifier (TastePROBE, Syntech, Hilversum, The Netherlands), and the signals
568 were collected and amplified (10x) by using a signal-connection interface box
569 (Syntech) in conjunction with a 100-3000 Hz band-pass filter. Action potential
570 measurements were acquired with a 9.6 kHz sampling rate and analyzed with
571 AutoSpike.
572 **RNA extraction, cDNA synthesis.** Total RNA from single flies of *D. mojavensis*
573 subspecies and from ~100 antennae was extracted using an RNA isolation kit (Direct-
574 zol™ RNA MiniPrep, Zymo Research). First strand cDNA was generated from 1.0 µg
575 of total RNA, using oligo-dT_{20} primers and SuperScript™ III (Thermo Fisher Scientific).
576 Derived cDNAs were used to amplify housekeeping and olfactory receptor open

577 reading frames via PCR with MyTaq™ DNA Polymerases (Bioline) and primers listed
578 in table S1. PCR amplicons were cloned into pCR4-TOPO (Invitrogen) and verified by
579 sequencing.
580 **Sequence alignment.** Available (https://flybase.org) and new-obtained protein-coding
581 sequences of *Or65a* and *Or47b* were analyzed in Geneious (v11.0.5). Briefly, a
582 multiple sequence alignment was generated using the MAFFT (v7.309) tool with E-
583 INS-I parameters and scoring matrix 200 PAM / K=2 as previously described (*48*). The
584 final tree of *Or65a* orthologs was reconstructed using a maximum likelihood approach
585 with the GTR+G+I model of nucleotide substitution and 1000 rate categories of sites
586 in Fasttree (v2.1.5). The tree was visualized and processed in Geneious.
587 **Functional analysis of receptor genes in *Xenopus* oocytes.** Oocyte injections and
588 two-electrode voltage clamp recordings were described previously (*49*). Briefly, the
589 open reading frames of *D. moj. wrigelyi Or47b1*, *Or47b2*, *Or65a*, *Or67d*, *Or88a* and
590 *O*rco were amplified from *D. moj. wrigelyi* cDNA using primers (table S1) adding BamHI
591 (fwd) and XbaI (rev) restriction sites, and a Kozak sequence (GCCACC) immediately
592 upstream of the first ATG. The PCR products were digested with BamHI and XbaI and
593 sub-cloned into the expression vector pCS2+. Maxi preps of recombinant plasmids
594 were linearized with NotI and transcribed to cRNAs with mMESSAGE mMACHINE
595 SP6 kit (Thermo Fisher Scientific, Waltham, MA, USA). *X. laevis* (purchased from
596 Xenopus Express France, Vernassal, Haute-Loire, France) oocytes were defolliculated
597 with 1.5 mg/mL collagenase (Sigma-Aldrich Co., St. Louis, MO, USA) in Oocyte Ringer
598 2 solution (82.5 mM NaCl, 2 mM KCl, 1 mM $MgCl_2$, 5 mM HEPES, pH 7.5). cRNAs of
599 each *Or* together with *D. moj. wrigelyi Orco* cRNA (50 ng each) were co-injected into
600 the oocytes and incubated at 18°C for 3-5 days prior to recordings. Stock solutions of
601 the tested compounds were prepared in dimethyl sulfoxide (DMSO) (Sigma-Aldrich
602 Co., St. Louis, MO, USA) and diluted to the indicated concentrations with Ringer's
603 buffer (96 mM NaCl, 2 mM KCl, 5 mM $MgC1_2$, 0.8 mM $CaCl_2$, 5 mM HEPES, pH 7.6).
604 The compounds mentioned in table S1 were applied to the oocytes successively at a
605 rate of 2 ml/min with extensive washings by Ringer's buffer in the intervals. Whole-cell
606 inward currents were recorded by two-electrode voltage clamp with a TEC-03BF
607 amplifier (npi electronic GmbH, Tamm, Germany) at the holding potential of -80 mV.
608 Data were collected and analyzed by Cellworks software (npi electronic GmbH, Tamm,
609 Germany).
610 **Expression of olfactory receptors in *D. melanogaster* at1 neurons.** Transgenic
611 lines were generated according to standard procedures as described (*50*). The open
612 reading frames of *D. moj. wrigelyi Or47b1, Or47b2, Or65a, Or67d, Or88a* and *D. moj.*
613 *sonorensis Or65a* receptors were subcloned from the corresponding pCS2+ constructs
614 (see above) via digestion with BamHI (Cat.# R0136, New England Biolabs) and XbaI
615 (Cat.#R0145 New England Biolabs) and ligated into pUASt.attb (*51*) (a gift from Dr.
616 Johannes Bischof) digested with BglII (Cat.#R0144, New Englands Biolabs) and XbaI
617 (Cat.#R0145, New England Biolabs). Homozygous *UAS-OrX* lines (with transgene
618 insertions into chromosome II) were generated at Bestgene
619 (https://www.thebestgene.com). An *Or67d*^{GAL4} stock (*12*) (provided by Dr. Barry J.
620 Dickson) was individually crossed to each of the transgenic *UAS-D. moj.-OrX* flies, and
621 homozygous lines expressing the Or gene of interest in the decoder at1 neuron of *D.*

622 *melanogaster* were established. Each *UAS*-transgenic line was confirmed by
623 sequencing of genomic DNA prepared from the final stocks.
624
625 **Generation of knock-out flies**
626 ***Drosophila* microinjections.** Transgenesis of *D. mojavensis wrigleyi* was performed
627 in-house following standard protocols (http://gompel.org/methods). For egg-laying
628 agar plates a few g of Formula 4-24® Instant *Drosophila* Medium, Blue (Carolina
629 Biological Supply Company) soaked in water were added on the surface. Embryos
630 were manually selected for the appropriate developmental stage prior to alignment and
631 injection. For CRISPR/Cas9-mediated genome engineering a mix of two sgRNAs (see
632 table S1 for sequences) targeting the *white* locus (to easily visualize a successful
633 genome editing event), two sgRNAs targeting the *Or65a* locus (3 µM each) and Cas9
634 protein (2 µM) (all Synthego; sgRNAs with 2'-O-methyl 3' phosphorothioate
635 modifications in the first and last 3 nucleotides) was prepared. Prior to injection
636 individual sgRNAs were mixed with Cas9 protein (1.5:1) and incubated at room
637 temperature for 10 min. All concentrations are the final values in the injection mix.
638 **Genotyping.** Individual G0 flies were crossed to wildtype flies and G1 adults visually
639 screened for white-eyed flies. Single white-eyed flies were subsequently crossed to
640 wildtype flies and G2 flies genotyped by PCR. Genomic DNA of a single wing of each
641 fly was isolated using the MyTaq™ Extract-PCR Kit (Bioline Cat No: BIO-21126), the
642 sgRNA-target site PCR amplified (see table S1 for genotyping primers) and the
643 amplicon Sanger-sequenced. Sequencing results were compared to the reference
644 sequence using TIDE (*52*) to deconvolute sequencing traces. G2 flies, which displayed
645 heterozygous loss-of-function mutations at the *Or65a* or white locus, were in-crossed
646 and independent stocks of *Or65a* and *white* loss-of-function alleles established. White-
647 eyed flies were not used in behavioural experiments as they might exhibit lower levels
648 of sexual activity.
649
650 **Histology and antennal lobe reconstruction**
651 **RNA *in situ* hybridizations.** RNA *in situ* hybridization on whole-mount antennae was
652 performed as previously described (*23*). In brief, both sense and antisense digoxigenin
653 (DIG) RNA probes were generated for each *Or* gene using a DIG-RNA labeling kit
654 (Roche, Indianapolis, IN, USA) according to manufacturer's instructions. See table S1
655 for details about the oligonucleotides' sequences. RNA probes were hydrolysed (60
656 mM Na_2CO_3, 40 mM $NaHCO_3$, pH 10.2) at 60°C for 1 h, ethanol precipitated and stored
657 in formamide at -80°C until use. Heads of *D. moj. wrigleyi* and *D. moj. sonorensis*
658 females were cold fixed (4% paraformaldehyde (PFA), 0.05% Tween 20 in 1× PBS)
659 for 1 h and then washed 3× 10 min in PBST (1× PBS, 0.1% Tween 20). Third antennal
660 segments were dissected into cold fix, washed 3× 10 min in PBX (1× PBS, 1% Triton-
661 X) and incubated for 2 h in hybridization (Hyb) buffer (50% formamide, 5× SSC, 0.05
662 mg/mL heparin, 0.1% Tween 20). Antennae were hybridized overnight at 55°C using
663 appropriate RNA probe(s) and the next day washed 5× 2 h in Hyb buffer at 55°C, with
664 the last wash leading to overnight incubation at 55°C. A wash of 20 min in Hyb buffer
665 at 55°C, and 3× 10 min wash in PBST at room temperature were subsequently

666 performed. Antennae were incubated in 1:500 anti-DIG-POD (in PBST and 1× BSA)
667 for 3 h followed by 3× 10 min wash in PBST. Samples were then incubated in TSA-
668 Plus Cyanine 5 (Cy5) according to manufacturer instruction (Perkin Elmer, Waltham,
669 MA, USA) for 70 min followed by 5× 10 min washes in PBST. Samples were
670 subsequently suspended in 80% glycerol for visualization using confocal microscopy.
671 Confocal Z-stacks were acquired using a Nikon A1Rsi inverted confocal microscope.
672 ORNs were counted using NIS Elements Viewer (Melville, NY, USA).
673 **Antennal lobe reconstruction.** Fly brain dissections and stainings were performed
674 as described previously (*33, 53*) with some modifications as follow: Brains were
675 dissected in PBS and fixed in 4% PFA for 30 min at room temperature (RT), rinsed 3×
676 15 min in PBS with 0.3% Triton X-100 (PT), followed by incubation with mouse
677 monoclonal nc82 antibody (1:30, CiteAb, A1Z7V1) in 4% normal goat serum (NGS,) in
678 PT (48 h at 4°C). Samples were washed 4× 20 min in PT, incubated overnight with
679 Alexa633-conjugated anti-mouse antibody (1:250, A21052, Invitrogen) in NGS-PT,
680 rinsed 4× 20 min in PT and mounted in Vectashield (Vector Laboratories). Images were
681 acquired with a Zeiss 710 NLO Confocal microscope using a 40× or 63× water
682 immersion objective. Reconstruction of whole antennal lobes and of individual
683 glomeruli (4-6 antennal lobes for each sex/species) was performed manually using the
684 segmentation software AMIRA version 5.6.0 (FEI Visualization Sciences Group).
685 Landmark glomeruli (DA1, DL3, VL2p, VL2a, VL1 and V) were labeled according to
686 their position based on the AL atlas of *D. melanogaster* (16) in order to compare
687 antennal lobes of *D. mojavensis* and *D. melanogaster* as previously done for a variety
688 of non-melanogaster species (*54*). Glomerular volume was calculated from
689 reconstructed glomeruli using the information on voxel size from the laser scanning
690 microscopy scans.
691 **OSN backfilling.** Trichoid sensilla in *D. mojavensis* were identified by SSR using
692 diagnostic odor-evoked responses to R-HDEA for at4 or *c*VA for at1. After identifying
693 the right sensillum, the recording electrode was removed and neurons were backfilled
694 by placing the sensillum inside a glass capillary filled with neurobiotin (Invitrogen, 2%
695 w/v in 0.25 M KCl). Neurobiotin was allowed to diffuse into the OSNs for 2 h. Brain
696 staining was performed as described above, and neurobiotin was visualized using
697 streptavidin conjugated to Alexa Fluor 555 (1:500, S32355, Invitrogen).
698 Due to its position we name the additional glomerulus innervated by *D. mojavensis* at4
699 neurons VA8. VA8 is located ventrally to VA1v and anterior to VL2a in an area that is
700 distant from the DL3 glomerulus targeted by at4 neurons in *D. melanogaster*.
701 **Scanning Electron Microscopy**. Antennal scans were performed as previously
702 described (*33*). Images of the third antennal segment were acquired at 4.5k×
703 magnification using a LEO 1450 VP scanning electron microscope with 10 kV and 11
704 mm working distance (Carl Zeiss).
705
706 **Phylogenetic analysis, statistics and figure preparation**
707 **Phylogenetic analysis.** The phylogenetic relationship among the four *D. mojavensis*
708 subspecies and other *Drosophila* species was determined using the recent genomic
709 analysis of *D. mojavensis* (*22*) and the *D. virilis, D. grimshawi, D. willistoni, D.*

710 *pseudoobscura, D. ananassae, D. yakuba, D. simulans*, and *D. melanogaster* FlyBase
711 assemblies (FB2019_04). The BUSCO application (*55*) was ran using the Diptera
712 dataset (composed of 2,799 loci) for all five genomes and a common set of 2,177 loci
713 was obtained. Individual gene alignments using MUSCLE (*56*) were then concatenated
714 and third base nucleotide positions (1,778,212 sites) were extracted. This dataset was
715 subsequently ran on FastTree (v2.1.10) (*57*) with the default CAT approximation with
716 20 rate categories under a GTR +G model and 1,000 bootstraps to assess the support
717 for the phylogenetic inference. For the receptor phylogeny, a multiple sequence
718 alignment was generated using the MAFFT (v7.309) tool with E-INS-I parameters and
719 scoring matrix 200 PAM / K=2 (*48*). The final tree was reconstructed using a maximum
720 likelihood approach with the GTR+G+I model of nucleotide substitution and 1000 rate
721 categories of sites in Fasttree (v2.1.5). The tree was visualized and processed in
722 Geneious (v11.0.5).
723 **Statistics and figure preparation.** Normality was first assessed on datasets using a
724 Shapiro test. Statistical analyses (see the corresponding legends of each figure) and
725 preliminary figures were conducted using GraphPad Prism v. 8
726 (https://www.graphpad.com). Figures were then processed with Adobe Illustrator CS5.
727
728 **References**

729 1. M. G. Ritchie, Sexual Selection and Speciation. *Annual Review of Ecology, Evolution,*
730 *and Systematics* **38**, 79-102 (2007).
731 2. O. Seehausen *et al.*, Speciation through sensory drive in cichlid fish. *Nature* **455**, 620-
732 626 (2008).
733 3. C. Smadja, R. K. Butlin, On the scent of speciation: the chemosensory system and its
734 role in premating isolation. *Heredity* **102**, 77-97 (2009).
735 4. H. T. Spieth, Courtship behavior in *Drosophila*. *Annu Rev Entomol* **19**, 385-405 (1974).
736 5. D. S. Manoli *et al.*, Male-specific fruitless specifies the neural substrates of *Drosophila*
737 courtship behaviour. *Nature* **436**, 395-400 (2005).
738 6. Y. Ding, A. Berrocal, T. Morita, K. D. Longden, D. L. Stern, Natural courtship song
739 variation caused by an intronic retroelement in an ion channel gene. *Nature* **536**,
740 329-+ (2016).
741 7. O. M. Ahmed *et al.*, Evolution of mechanisms that control mating in *Drosophila*
742 males. *Cell Rep* **27**, 2527-2536 e2524 (2019).
743 8. L. F. Seeholzer, M. Seppo, D. L. Stern, V. Ruta, Evolution of a central neural circuit
744 underlies *Drosophila* mate preferences. *Nature* **559**, 564-+ (2018).
745 9. M. R. E. Symonds, B. Wertheim, The mode of evolution of aggregation pheromones
746 in *Drosophila* species. *J Evolution Biol* **18**, 1253-1263 (2005).
747 10. T. O. Auer, R. Benton, Sexual circuitry in *Drosophila*. *Curr Opin Neurobiol* **38**, 18-26
748 (2016).
749 11. S. Guo, J. Kim, Molecular evolution of *Drosophila* odorant receptor genes. *Mol Biol*
750 *Evol* **24**, 1198-1207 (2007).
751 12. A. Kurtovic, A. Widmer, B. J. Dickson, A single class of olfactory neurons mediates
752 behavioural responses to a *Drosophila* sex pheromone. *Nature* **446**, 542-546 (2007).

753 13. H. K. M. Dweck *et al.*, Pheromones mediating copulation and attraction in *Drosophila*.
754 *Proceedings of the National Academy of Sciences of the United States of America* **112**,
755 E2829-E2835 (2015).
756 14. W. W. Liu *et al.*, Social regulation of aggression by pheromonal activation of Or65a
757 olfactory neurons in *Drosophila*. *Nat Neurosci* **14**, 896-U119 (2011).
758 15. A. Ejima *et al.*, Generalization of courtship learning in *Drosophila* is mediated by cis-
759 vaccenyl acetate. *Curr Biol* **17**, 599-605 (2007).
760 16. V. Grabe, A. Strutz, A. Baschwitz, B. S. Hansson, S. Sachse, Digital in vivo 3D atlas of
761 the antennal lobe of *Drosophila melanogaster*. *J Comp Neurol* **523**, 530-544 (2015).
762 17. A. Couto, M. Alenius, B. J. Dickson, Molecular, anatomical, and functional
763 organization of the *Drosophila* olfactory system. *Curr Biol* **15**, 1535-1547 (2005).
764 18. L. M. Matzkin, Ecological genomics of host shifts in *Drosophila mojavensis*. *Ecological*
765 *Genomics: Ecology and the Evolution of Genes and Genomes* **781**, 233-247 (2014).
766 19. W. J. Etges, Evolutionary genomics of host plant adaptation: insights from *Drosophila*.
767 *Curr Opin Insect Sci* **36**, 96-102 (2019).
768 20. E. Pfeiler, S. Castrezana, L. K. Reed, T. A. Markow, Genetic, ecological and
769 morphological differences among populations of the cactophilic *Drosophila*
770 mojavensis from southwestern USA and northwestern Mexico, with descriptions of
771 two new subspecies. *J Nat Hist* **43**, 923-938 (2009).
772 21. A. Ruiz, W. B. Heed, M. Wasserman, Evolution of the *mojavensis* cluster of cactophilic
773 *Drosophila* with descriptions of 2 new species. *J Hered* **81**, 30-42 (1990).
774 22. C. W. Allan, L. M. Matzkin, Genomic analysis of the four ecologically distinct cactus
775 host populations of *Drosophila mojavensis*. *Bmc Genomics* **20**, 732 (2019).
776 23. A. Crowley-Gall *et al.*, Population differences in olfaction accompany host shift in
777 *Drosophila mojavensis*. *P Roy Soc B-Biol Sci* **283**, (2016).
778 24. B. D. Newby, W. J. Etges, Host preference among populations of *Drosophila*
779 *mojavensis* (Diptera : Drosophilidae) that use different host cacti. *J Insect Behav* **11**,
780 691-712 (1998).
781 25. L. L. Knowles, T. A. Markow, Sexually antagonistic coevolution of a postmating-
782 prezygotic reproductive character in desert *Drosophila*. *P Natl Acad Sci USA* **98**, 8692-
783 8696 (2001).
784 26. T. A. Markow, Sexual isolation among populations of *Drosophila mojavensis*.
785 *Evolution* **45**, 1525-1529 (1991).
786 27. W. J. Etges, M. A. Ahrens, Premating isolation is determined by larval-rearing
787 substrates in cactophilic *Drosophila mojavensis*. V. Deep geographic variation in
788 epicuticular hydrocarbons among isolated populations. *Am Nat* **158**, 585-598 (2001).
789 28. S. Zawistowski, R. C. Richmond, Inhibition of courtship and mating of *Drosophila*
790 *melanogaster* by the male-produced lipid, cis vaccenyl acetate. *J. Insect Physiol* **32**,
791 189–192 (1986).
792 29. J. Y. Yew *et al.*, A New Male Sex pheromone and novel cuticular cues for chemical
793 communication in *Drosophila*. *Current Biology* **19**, 1245-1254 (2009).

794 30. W. V. G. van Naters, J. R. Carlson, Receptors and neurons for fly odors in *Drosophila*.
795 *Curr Biol* **17**, 606-612 (2007).
796 31. L. L. Prieto-Godino *et al.*, Evolution of acid-sensing olfactory circuits in Drosophilids.
797 *Neuron* **93**, 661-+ (2017).
798 32. T. O. Auer *et al.*, Olfactory receptor and circuit evolution promote host specialization.
799 *Nature*, (2020).
800 33. V. Grabe *et al.*, Elucidating the neuronal architecture of olfactory glomeruli in the
801 *Drosophila* antennal lobe. *Cell Rep* **16**, 3401-3413 (2016).
802 34. W. J. Etges, K. F. Over, C. C. De Oliveira, M. G. Ritchie, Inheritance of courtship song
803 variation among geographically isolated populations of *Drosophila mojavensis. Anim*
804 *Behav* **71**, 1205-1214 (2006).
805 35. J. S. R. Chin *et al.*, Sex-specific triacylglycerides are widely conserved in *Drosophila*
806 and mediate mating behavior. *Elife* **3**, (2014).
807 36. J. Kohl, P. Huoviala, G. S. X. E. Jefferis, Pheromone processing in *Drosophila*. *Curr Opin*
808 *Neurobiol* **34**, 149-157 (2015).
809 37. V. Ruta *et al.*, A dimorphic pheromone circuit in *Drosophila* from sensory input to
810 descending output. *Nature* **468**, 686-U106 (2010).
811 38. P. M. O'Grady, T. A. Markow, Rapid morphological, behavioral, and ecological
812 evolution in *Drosophila*: comparisons between the endemic Hawaiian *Drosophila* and
813 the cactophilic repleta species group. *Rapidly Evolving Genes and Genetic Systems* **1**,
814 176-186 (2012).
815 39. D. Mercier, Y. Tsuchimoto, K. Ohta, H. Kazama, Olfactory landmark-based
816 communication in interacting *Drosophila*. *Curr Biol* **28**, 2624-+ (2018).
817 40. S. Lebreton *et al.*, Love makes smell blind: mating suppresses pheromone attraction
818 in *Drosophila* females via Or65a olfactory neurons. *Sci Rep-Uk* **4**, (2014).
819 41. I. W. Keesey *et al.*, Inverse resource allocation between vision and olfaction across
820 the genus *Drosophila*. *Nat Commun* **10**, 1162 (2019).
821 42. J. Stokl *et al.*, A deceptive pollination system targeting Drosophilids through olfactory
822 mimicry of yeast. *Curr Biol* **20**, 1846-1852 (2010).
823 43. F. Kaftan *et al.*, Mass spectrometry imaging of surface lipids on intact *Drosophila*
824 *melanogaster* flies. *J Mass Spectrom* **49**, 223-232 (2014).
825 44. P. Horka, V. Vrkoslav, R. Hanus, K. Peckova, J. Cvacka, New MALDI matrices based on
826 lithium salts for the analysis of hydrocarbons and wax esters. *J Mass Spectrom* **49**,
827 628-638 (2014).
828 45. P. Date *et al.*, Divergence in olfactory host plant preference in *D. mojavensis* in
829 response to cactus host use. *Plos One* **8**, (2013).
830 46. S. B. Olsson, B. S. Hansson, Electroantennogram and single sensillum recording in
831 insect antennae. *Methods Mol Biol* **1068**, 157-177 (2013).
832 47. S. J. Moon, M. Köttgen, Y. Jiao, H. Xu, C. Montell, A taste receptor required for the
833 caffeine response in vivo. *Curr Biol* **16**, 1812-1817 (2006).
834 48. K. Katoh, D. M. Standley, MAFFT multiple sequence alignment software version 7:
835 improvements in performance and usability. *Mol Biol Evol* **30**, 772-780 (2013).

49. D. D. Zhang, C. Lofstedt, Functional evolution of a multigene family: orthologous and paralogous pheromone receptor genes in the turnip moth, *Agrotis segetum*. *Plos One* **8**, (2013).
50. F. Gonzalez, P. Witzgall, W. B. Walker, Protocol for heterologous expression of insect odourant receptors in *Drosophila*. *Frontiers in Ecology and Evolution* **4**, (2016).
51. J. Bischof, R. K. Maeda, M. Hediger, F. Karch, K. Basler, An optimized transgenesis system for *Drosophila* using germ-line-specific phi C31 integrases. *P Natl Acad Sci USA* **104**, 3312-3317 (2007).
52. E. K. Brinkman, T. Chen, M. Amendola, B. van Steensel, Easy quantitative assessment of genome editing by sequence trace decomposition. *Nucleic Acids Res* **42**, e168 (2014).
53. T. Dekker, I. Ibba, K. P. Siju, M. C. Stensmyr, B. S. Hansson, Olfactory shifts parallel superspecialism for toxic fruit in *Drosophila melanogaster* sibling, *D. sechellia*. *Curr Biol* **16**, 101-109 (2006).
54. Y. Kondoh, K. Y. Kaneshiro, K. Kimura, D. Yamamoto, Evolution of sexual dimorphism in the olfactory brain of Hawaiian *Drosophila*. *P Roy Soc B-Biol Sci* **270**, 1005-1013 (2003).
55. R. M. Waterhouse *et al.*, BUSCO Applications from quality assessments to gene prediction and phylogenomics. *Mol Biol Evol* **35**, 543-548 (2018).
56. R. C. Edgar, MUSCLE: multiple sequence alignment with high accuracy and high throughput. *Nucleic Acids Res* **32**, 1792-1797 (2004).
57. M. N. Price, P. S. Dehal, A. P. Arkin, FastTree 2-approximately maximum-likelihood trees for large alignments. *Plos One* **5**, (2010).
58. T. A. Markow, Evolution of *Drosophila* mating systems. *Evol Biol* **29**, 73–106 (1996).
59. L. L. Prieto-Godino *et al.*, Functional integration of “undead” neurons in the olfactory system. *Science Advances* **6**, eaaz7238 (2020).
60. G. W. Francis, Alkylthiolation for the determination of double-bond position in unsaturated fatty-acid esters. *Chem Phys Lipids* **29**, 369-374 (1981).
61. A. V. R. Rao, D. R. Reddy, A simple methodology for the synthesis of 3,4-dihydroisocoumarins. *Synthetic Commun* **16**, 97-102 (1986).

Acknowledgements: We thank R. Stieber for performing immunohistochemistry experiments, I. Alali for fly rearing and maintenance, L. Zhang for the preliminary molecular data, and J. Layne for his technical help in confocal imaging. We are grateful to K. Weniger, Sybille Lorenz, S. Trautheim, C. Hoyer and L. Merkel for their technical support, and to J.R. Arguello, L. Prieto-Godino, W.B. Walker III and members of the Department of Evolutionary Neuroethology, MPI-CE, in Jena, Germany for discussions. Transgenic flies were obtained from the Bloomington *Drosophila* Stock Center (NIH P40OD018537), and wild-type flies were obtained from the San Diego *Drosophila* Species Stock Center (now The National *Drosophila* Species Stock Center, Cornell University).
Funding: This research was supported through funding by the Max Planck Society.

T.O.A. is supported by a Human Frontier Science Program Long-Term Fellowship (LT000461/2015-L). B.A. is supported by a National Science Foundation grant (IOS-1456932). D.Z and C.L are supported by the Royal Physiographic Society of Lund and the Swedish Research Council. L.M.M. lab was partly supported by a National Science Foundation grant (IOS-1557697). Research in R.B.'s laboratory is supported by ERC Consolidator and Advanced Grants (615094 and 833548, respectively).

Author Contributions: M.A.K, H.K.M.D., B.S.H., and M.K. conceived of the project. All authors contributed to experimental design, analysis and interpretation of results. M.A.K. prepared all figures. M.A.K. with the help of T.O.A. designed the genetic constructs and T.O.A. performed the microinjections for new drosophilid mutants. S.L generated reagents for the transgenic flies. A.S. identified and J.W. synthesized the novel compounds. Other experimental contributions were as follows: M.A.K (Fig.1, Fig.2, Fig. 3, Fig. 4, Fig. 5C, E-J' and L, Fig. 6, fig. S1, fig. S2A-C and F-G, fig. S3, fig. S4, fig. S5A and C-G, fig. S6B, D-F, fig. S7, movies S1-4 and 7-9, and data file S1), T.O.A (Fig. 5H), V.G and A.D (Fig. 5K-M, fig. S6A-E and F-G and movies S5-9), B.A. (Fig. 5A-B), D.Z. and C.L. (Fig. 5D and fig. S5B), F.K. (fig. S2B-C), L.M.M. (Fig. 1B, fig. S1A and fig. S6D). M.A.K. wrote the original manuscript, and M.K., T.O.A, R.B. and B.S.H. contributed to the final manuscript. All coauthors contributed to the subsequent revisions.

Competing interests: the authors declare that they have no competing interests.
Data and biological material availability: All relevant data supporting the findings of this study and all unique biological materials generated in this study (e.g., mutant and transgenic fly strains) are available from the corresponding authors upon request.

922 **FIGURE LEGENDS**

923 **Fig. 1. Sexual isolation among *D. mojavensis* subspecies.**

924 **(A)** Geographic distribution of *D. mojavensis* subspecies on the west coast of North
925 America. Pink, *D. moj. wrigleyi*; orange, *D. moj. mojavensis*; turquoise, *D. moj.*
926 *sonorensis*; violet, *D. moj. baja*; adapted from (*20*).

927 **(B)** Phylogenetic relationship of *D. mojavensis* subspecies based on concatenated
928 sequences of 9087 genes available from (*22*) (See fig. S1A and Materials and Methods
929 for details). Scale bar for branch length represents the number of substitutions per site.
930 Bootstrap values are indicated by the numbers at the nodes.

931 **(C)** Top row: Competition mating arenas where a female of each *D. mojavensis*
932 subspecies had the choice to mate with a con-subspecific male or a male of one of the
933 other three subspecies (color coded as in Fig. 1A). Below: Pie-charts represent the
934 percentages of copulation success of the rival males. Ns $P > 0.05$; ** $P < 0.01$; *** $P <$
935 0.001, chi-square test (*n* from left column to right column = 84, 84, 76, 52, 84, 80, 88,
936 68, 92, 80, 72, and 64 replicates). See fig. S1B for details regarding the differences
937 and similarities of sexual behaviors among the four subspecies and fig. S1I for details
938 on the competition preference indices of males between con-subspecific and hetero-
939 subspecific females.

940

941 **Fig. 2. Distinct, but overlapping, male-specific compounds of *D. mojavensis***
942 **subspecies.**

943 **(A)** Representative gas chromatograms of 10 day old male (virgin, ♂) and female flies
944 (virgin; v♀ and mated; m♀) (*n* = 7) obtained by solvent-free thermal desorption-gas
945 chromatography-mass spectrometry (TD-GC-MS) (*13*). Colored peaks indicate the
946 male-specific compounds (see Materials and Methods for chemical syntheses), which
947 are transferred to females during mating. Red: R and S enantiomers of (*Z*)-10-
948 Heptadecen-2-yl acetate (R&S-HDEA); blue: heptadec-2yl acetate (HDA); light green:
949 (*Z,Z*)-19,22-octacosadien-1yl acetate (OCDA). Different colored backgrounds
950 represent the different subspecies (similar to Fig. 1A). Unless otherwise noted, in this
951 and other panels *D. moj. wrigleyi* (15081-1352.22), *D. moj. mojavensis* (15081-
952 1352.47), *D. moj. sonorensis* (15081-1351.01), and *D. moj. baja* (15081-1351.04) were
953 used. Two more strains of each subspecies (see table S1 for details) were analyzed
954 showing very similar profiles (fig. S2A'). See fig. S2A for details regarding the body
955 wash extracts analyzed by GC-MS.

956 **(B)** Summary table of the different male-transferred compounds of all *D. mojavensis*
957 subspecies.

958 **(C)** Amount of the male-specific compounds and corresponding copulation
959 performance. Colored bars and error bars indicate mean amounts and SEM of the
960 three male-specific acetates (*n* = 3 males per age); grey dashes indicate the
961 percentage of copulation success for males of the same age within a 10 min time
962 window (*n* = 20 males per age). See fig. S2F for the production site of these male-
963 specific compounds.

964

965 **Fig. 3. Conserved behavioral responses among *D. mojavensis* subspecies to**
966 **OCDA.**

967 **(A)** Top: Schematic of courtship arena where a dead (virgin or mated) female (*D. moj.*
968 *wrigleyi* and *D. moj. sonorensis*) was presented to a con-subspecific male. Below, y-
969 axis represents courtship index [%] (equal the time a male exhibits courtship behaviors
970 (fig. S1B) / total amount of recording time (10 min)). In this and other panels, filled
971 circles indicate significant difference between the tested groups; * $P < 0.05$; ** $P < 0.01$,
972 Mann Whitney U test ($n = 40$). Males and females used in this and other panels are 10
973 days old.
974 **(B)** Top: Schematic of a male courting a dead virgin female of the same subspecies
975 perfumed with hexane as a control (black) or OCDA diluted in hexane (light green).
976 Kruskal-Wallis test between different treatments (fig. S3A) with Dunn's post-hoc
977 correction. Ns $P > 0.05$; * $P < 0.05$; ** $P < 0.01$ ($n = 40$ assays). See fig. S3A for the
978 role of the other male-specific acetates in male courtship suppression in both
979 subspecies.
980 **(C)** Left top: micrograph of tarsal segments of the foreleg showing different sensory
981 hairs. Scale bar = 50 µm. Right top: schematics of tip recordings from the foreleg tarsal
982 sensillum (class 5b). Bottom: tip recording measurements from foreleg-tarsi of *D. moj.*
983 *wrigleyi* and *D. moj. sonorensis* males using DMSO or OCDA. Kruskal-Wallis test
984 between different treatments (fig. S3D) with Dunn's post-hoc correction. Ns $P > 0.05$;
985 ** $P < 0.01$ ($n = 5$). See fig. S3C for tip recording traces and fig. S3D for
986 electrophysiological responses to the other male-specific acetates.
987 **(D)** Courtship indices of tarsi-less males tested with a dead virgin female of the same
988 subspecies perfumed with hexane (black) or OCDA (light green). Ns > 0.05, Mann
989 Whitney U test ($n = 20$ assays).
990
991 **Fig. 4. R-HDEA provokes divergent sexual behaviors through activation of**
992 **homologous sensory neurons.**
993 **(A)** Left: Schematic of mating arena where a perfumed male courts a virgin con-
994 subspecific female. Black droplet: hexane (control); grey droplet: one of the other three
995 male-transferred compounds. Right: Copulation success of *D. moj. wrigleyi* and *D. moj.*
996 *sonorensis* males perfumed with hexane or male-specific acetates. Fisher exact test.
997 Ns $P > 0.05$ ($n = 40$ assays per treatment). See fig. S4A for OCDA impact on copulation
998 success and fig. S3E for courtship indices of hexane and acetates-perfumed males
999 toward females of the same subspecies.
1000 **(B)** Copulation latencies of the same males as in Fig. 4A. Filled circles indicate
1001 significant differences from the solvent. Kruskal-Wallis test with Dunn's post-hoc
1002 correction. Ns $P > 0.05$; * $P < 0.05$ (n from left to right (the number of successful
1003 copulations in Fig. 4A) = 29, 28, 29, 24, 32, 28, 30, and 26 assays). See fig. S4B for
1004 OCDA impact on females' copulation latencies.
1005 **(C)** Competition between two con-subspecific males, perfumed with one of the three
1006 compounds (colored droplet) or with the solvent hexane (black droplet), to copulate
1007 with a virgin female of the same subspecies. Pie-charts represent copulation success
1008 of the rival males. Filled droplets indicate significant difference between the tested
1009 groups. Chi-square test, ns $P > 0.05$; ** $P < 0.01$, from top to bottom = 124, 120, 124,
1010 104, 112, and 116 assays. See fig. S4C for the competition results of OCDA-perfumed
1011 males and fig. S4D for *D. moj. mojavensis* and *D. moj. baja* competition experiments.

1012 **(D)** Scanning electron micrograph of antennal surface showing different sensillum
1013 types (intermediate, trichoid, coeloconic and basiconic). Scale bar = 2 µm.
1014 **(E)** Electrophysiological responses towards R-HDEA, S-HDEA and HDA in all types of
1015 olfactory sensilla on antenna and maxillary palp of *D. moj. wrigleyi* (pink) and *D. moj.*
1016 *sonorensis* (turquoise). Mann Whitney U test, ns $P > 0.05$; *** $P < 0.001$ (n = 3-6
1017 neurons). ab, antennal basiconic; ac, antennal coeloconic; at, antennal trichoid; ai,
1018 antennal intermediate; pb, palp basiconic. See fig. S4, E and H for similarity between
1019 male and female responses to R-HDEA, OCDA responses, representative SSR traces,
1020 and responses of R-HDEA among *D. mojavensis* subspecies, respectively.
1021 **(F)** Dose-dependent responses of at4 neurons in *D. moj. wrigleyi* and *D. moj.*
1022 *sonorensis* toward R-HDEA (in red) and HDA (in blue) (Mean ± SEM). Two-way
1023 ANOVA followed by Sidek's multiple comparison test between the two subspecies'
1024 responses to the same stimulus, ns P > 0.05 (n = 4-6 neurons). See fig. S4I for *D.*
1025 *melanogaster* at1 and at4 responses to *D. moj. wrigleyi*-specific acetates and fig. S4J
1026 for alignments of *D. moj. wrigleyi*-OR65a and *D. melanogaster*-OR65a/b/c protein
1027 sequences.
1028
1029 **Fig. 5. Conserved peripheral sensory pathways for R-HDEA detection among *D.***
1030 ***mojavensis* subspecies.**
1031 **(A)** Expression of olfactory receptor genes (*OrX*: *Or47b*, *Or88a*, *Or65a* and *Or67d*) in
1032 *D. moj. wrigleyi and D. moj. sonorensis* female antennae. See Materials and Methods
1033 and fig. S5A for the receptor terminology. Due to the high degree of sequence identity
1034 (99.1%) of the *Or47b*-related loci (Data file S1), cross-hybridization between probes
1035 and mRNAs is likely to occur.
1036 **(B)** Number of the *Or*-expressing cells (*OrX*: *Or47b*, *Or88a*, *Or65a* and *Or67d*) in *D.*
1037 *moj. wrigleyi* and *D. moj. sonorensis* females. Filled circles indicate significant
1038 differences between both species. Mann Whitney U test, ns $P > 0.05$; * $P < 0.05$ (n =
1039 10 antennae).
1040 **(C)** Left: Schematic of voltage-clamp recordings from *Xenopus laevis* oocytes
1041 ectopically expressing the different odorant receptors (ORX) together with ORCO.
1042 **(D)** Electrophysiological responses of oocytes expressing different odorant receptor
1043 genes to R-HDEA (1mM). In this panel and Fig. 5F, filled circles indicate significant
1044 differences from the solvent response. Mann Whitney U test, ns $P > 0.05$; * $P < 0.05$;
1045 *** $P < 0.001$ (n = 4-8 recordings). See fig. S5B for details. Right: Traces of
1046 electrophysiological responses of *D. moj. wrigleyi*-OR65a to DMSO and R-HDEA.
1047 **(E)** Schematic of odorant receptors (ORX) expressed in *D. melanogaster* at1 neurons.
1048 **(F)** Electrophysiological responses of five odorant receptors expressed in *D.*
1049 *melanogaster* at1 neurons to R-HDEA (10 µg). Mann Whitney U test, ns $P > 0.05$; ***
1050 $P < 0.001$ (n = 7 recordings). See fig. S5C for details.
1051 **(G)** Electrophysiological responses of *D. moj. wrigleyi* or *D. moj. sonorensis* OR65a
1052 towards increasing concentrations of R-HDEA (n = 8 recordings). Two-way ANOVA
1053 followed by Sidek's multiple comparison test between the two subspecies' responses
1054 to the same stimulus, ns P > 0.05.
1055 **(H)** Schematics of the *D. moj. Or65a* locus illustrating the sgRNA binding sites.
1056 Scissors denote the presumed cutting site. The *Or65a* loss-of-function allele carries a

1057 2 bp deletion in exon 1, resulting in a premature stop codon (highlighted in red). See
1058 fig. S5, E and F for details on generating *white* gene knock-outs using CRISPR/Cas9.
1059 **(I)** Electrophysiological responses of *Or65a* heterozygous (left) and homozygous
1060 (right) animals to hexane, R-HDEA and methyl laurate (ML; diagnostic odor for OR47b
1061 and OR88a (*13*)). The latter shows an intact neuronal excitation of the Or65a-
1062 neighbouring neuron(s). See fig. S5D regarding quantification of SSR responses.
1063 **(J)** Competition between two males of *D. moj. wrigleyi*, perfumed with R-HDEA (red
1064 droplet) or hexane (black droplet), to copulate with a transgenic virgin female of the
1065 same subspecies. Left: Heterozygous animal at the *Or65a* locus (n = 148); right:
1066 homozygous mutant at the *Or65a* locus (n = 128). Filled droplets indicate a significant
1067 difference between the rival males. Chi-square test, ns $P > 0.05$; ** $P < 0.01$. All males
1068 and females used in this and other panels were 10-day-old virgin flies.
1069 **(J')** Copulation latencies in seconds (s) for *Or65a* heterozygous (left) and homozygous
1070 (right) females courted by wildtype males (single-pair assays). Filled circles indicate
1071 significant differences between both transgenic females. Mann Whitney U test, ns $P >$
1072 0.05; * $P < 0.05$ (n = 25).
1073 **(K)** Three-dimensional reconstruction of antennal lobes from representative female
1074 brains of *D. moj. wrigleyi* and *D. moj. sonorensis*. Neurobiotin-marked neurons in Fig.
1075 5L are highlighted: VA1d (green), VA1v (yellow), and VA8 (only present in *D. moj.*
1076 *wrigleyi* and *D. moj. sonorensis* in blue). Landmark glomeruli (DA1, DL3, VL2p, VL2a,
1077 VL1 and V glomeruli), highlighted in dark grey, are used to support the homology of
1078 these three glomeruli in both *D. mojavensis* subspecies. VA8 is located ventrally to
1079 VA1v and anterior to VL2a in an area far off the DL3 glomerulus, which targeted by
1080 Or65a neurons *in D. melanogaster*. See fig. S6, A to C for details. Scale bar = 20 µm.
1081 **(L)** Left top panel: Fluorescent staining for neurobiotin (magenta) and nc82 (grey) of
1082 *D. moj. wrigleyi* antennal lobe, backfilled from the at4 sensillum in *D. moj. wrigleyi*
1083 (identified by electrophysiological recordings; Fig. 4E). Right top panel: Reconstruction
1084 of the neurobiotin-marked neurons and their corresponding glomeruli reveals at4-
1085 housed neurons project to three glomeruli (*D. mojavensis* VA8, VA1v and VA1d). Left
1086 panel: Neurobiotin backfilled neurons from at4 sensillum in *D. moj. sonorensis* that
1087 innervate similar regions in antennal lobe. Images in the four panels correspond to a
1088 projection of 40 Z-stacks (Watch movies S7 and S8). Landmark glomeruli were labeled
1089 according to their positions based on the map of the *D. melanogaster* AL (*16*) (See
1090 Materials and Methods). See fig. S6, D to F and movie S9 for backfilling of at1 sensilla.
1091 **(M)** Volumes of VA1d, VA1v, and VA8 glomeruli normalized to the total antennal lobe
1092 volume in *D. moj. wrigleyi* and *D. moj. sonorensis* (males in black, females in grey).
1093 Filled circles indicate significant difference between both sexes of the same
1094 subspecies. Mann Whitney U test, ns $P > 0.05$; * $P < 0.05$ (n = 4-6 brains).
1095
1096 **Fig. 6. R-HDEA and auditory cues collaborate to define sexual isolation among**
1097 ***D. mojavensis* subspecies.**
1098 **(A)** Competition between two males of different subspecies to copulate with a *D. moj.*
1099 *wrigleyi* virgin female (n = 80). Pie-charts in A-C' represent copulation success [%] of
1100 the rival males. Chi-square test, ns $P > 0.05$; ** $P < 0.01$; *** $P < 0.001$. All males and
1101 females used in this and other panels were 10-day-old virgin flies.

(A') Competition between two males of different subspecies, *D. moj. sonorensis* perfumed with R-HDEA (red droplet) and *D. moj. wrigleyi* perfumed with hexane (black droplets), to copulate with a *D. moj. wrigleyi* virgin female (*n* = 108). See fig. S7A for details regarding the S-HDEA and HDA-perfumed males.

(A'') Competition between two males of *D. moj. sonorensis*, perfumed with R-HDEA (red droplet) or hexane (black droplet), to copulate with a *D. moj. wrigleyi* virgin female (*n* = 76).

(B) Competition between two males of different subspecies, *D. moj. sonorensis* and *D. moj. wrigleyi*, to copulate with a *D. moj. wrigleyi* virgin female that lacks the R-HDEA-detecting channel Or65a (*n* = 72).

(B') Competition between two aristaless males of different subspecies, *D. moj. sonorensis* and *D. moj. wrigleyi*, to copulate with an aristaless *D. moj. wrigleyi* virgin female (*n* = 48).

(B'') Competition between two aristaless males of different subspecies, *D. moj. sonorensis* and *D. moj. wrigleyi*, to copulate with an aristaless *D. moj. wrigleyi* virgin female that lacks the R-HDEA-detecting channel Or65a (*n* = 84).

(C) Competition between two males of different subspecies, *D. moj. sonorensis* perfumed with R-HDEA (red droplet) and *D. moj. wrigleyi* perfumed with hexane (black droplets), to copulate with a *D. moj. sonorensis* virgin female (*n* = 68) See fig. S7B for details regarding the S-HDEA and HDA-perfumed males.

(C') Competition between two aristaless males of different subspecies, *D. moj. sonorensis* and *D. moj. wrigleyi*, to copulate with an aristaless *D. moj. sonorensis* virgin female (*n* = 64).

Fig. 1

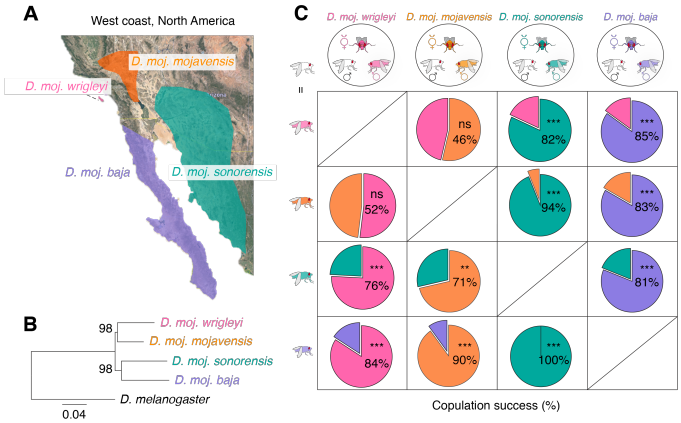

1128
1129
1130

Fig. 2

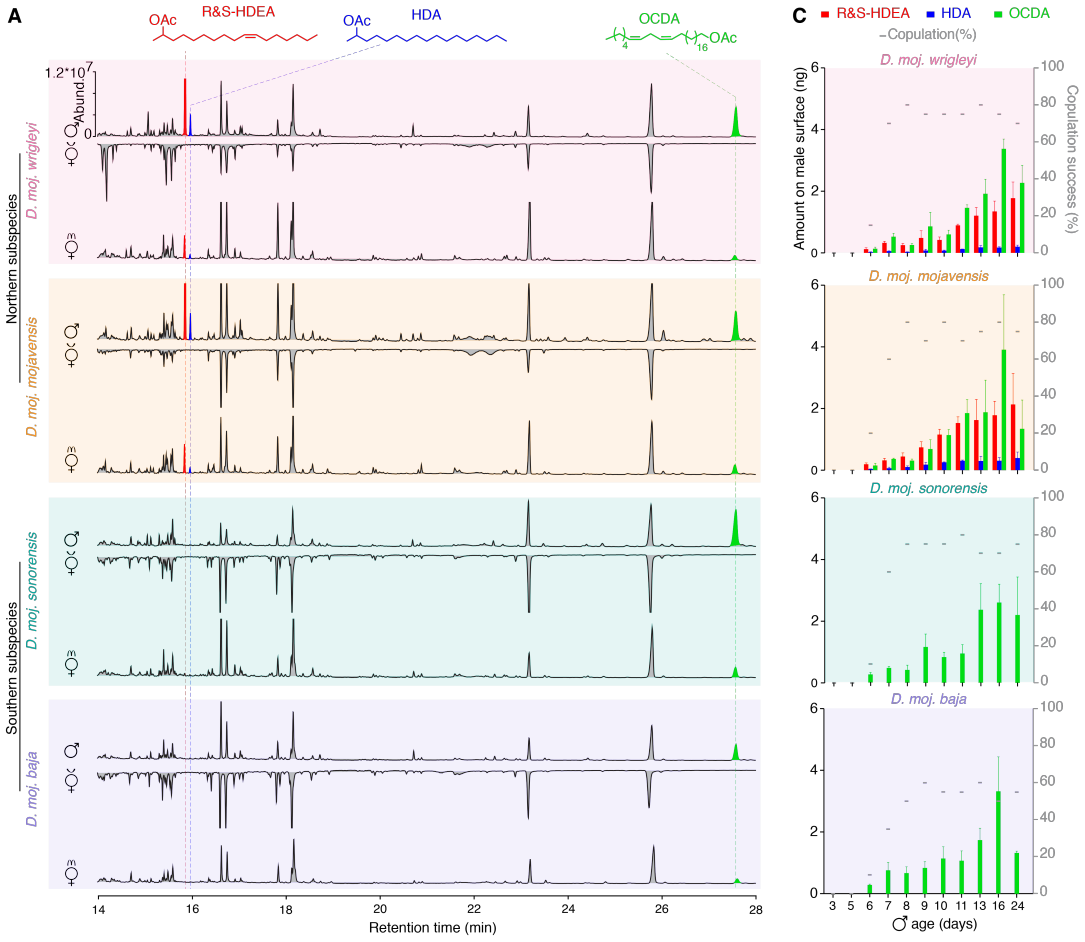

B

Male-transferred compounds	*D. moj. wrigleyi*	*D. moj. mojavensis*	*D. moj. sonorensis*	*D. moj. baja*
R/S-HDEA and HDA	+	+	–	–
OCDA	+	+	+	+

1131

Fig. 3

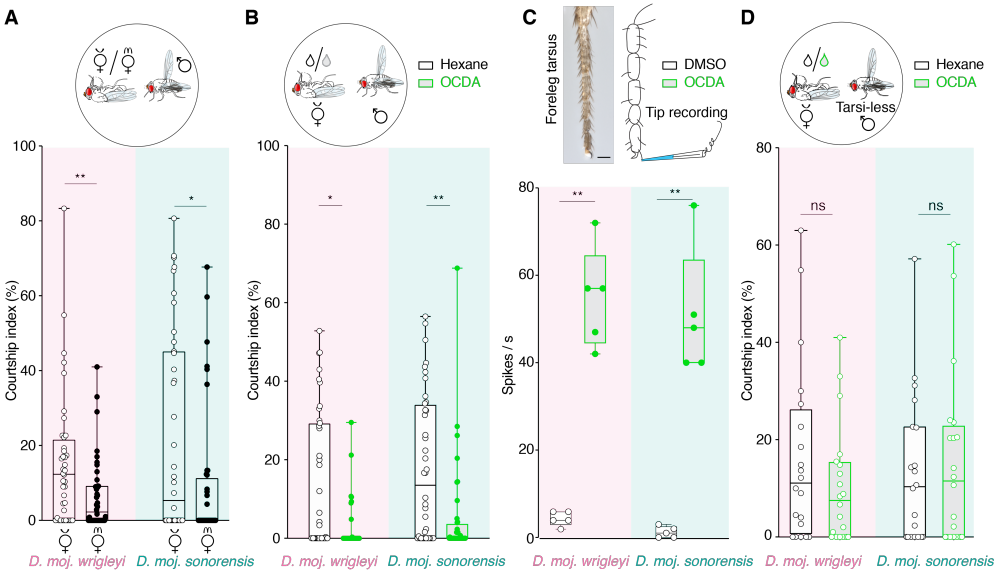

1132
1133

Fig. 4

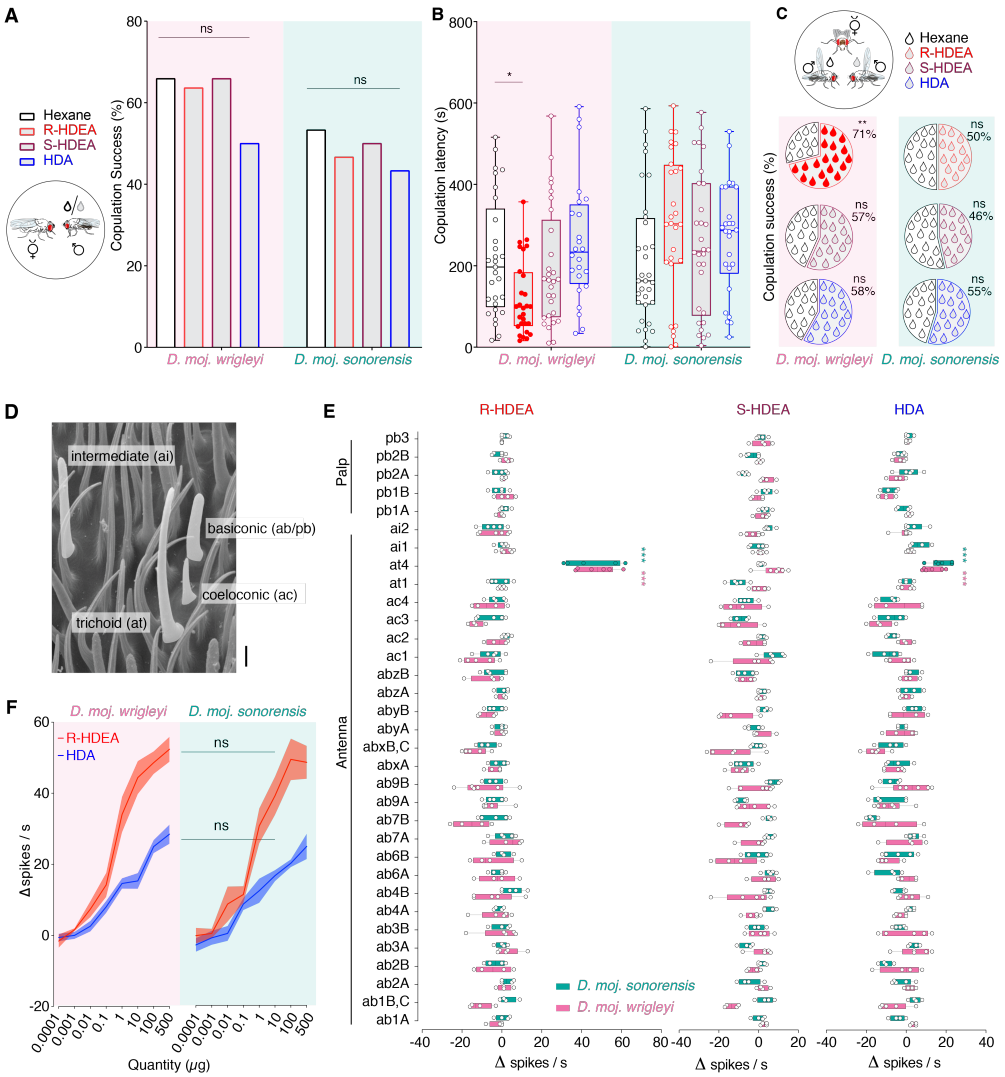
A
Hexane
R-HDEA
S-HDEA
HDA
Copulation Success (%)
ns
ns
D. moj. wrigleyi
D. moj. sonorensis
B
Copulation latency (s)
*
D. moj. wrigleyi
D. moj. sonorensis
C
Hexane
R-HDEA
S-HDEA
HDA
Copulation success (%)
** 71%
ns 57%
ns 58%
ns 50%
ns 46%
ns 55%
D. moj. wrigleyi
D. moj. sonorensis
D
intermediate (ai)
basiconic (ab/pb)
coeloconic (ac)
trichoid (at)
E
R-HDEA
S-HDEA
HDA
Palp
Antenna
pb3
pb2B
pb2A
pb1B
pb1A
ai2
ai1
at4
at1
ac4
ac3
ac2
ac1
abzB
abzA
abyB
abyA
abxB,C
abxA
ab9B
ab9A
ab7B
ab7A
ab6B
ab6A
ab4B
ab4A
ab3B
ab3A
ab2B
ab2A
ab1B,C
ab1A
D. moj. sonorensis
D. moj. wrigleyi
Δ spikes / s
F
D. moj. wrigleyi
D. moj. sonorensis
R-HDEA
HDA
ns
ns
Δspikes / s
Quantity (μg)

1134

Fig. 5

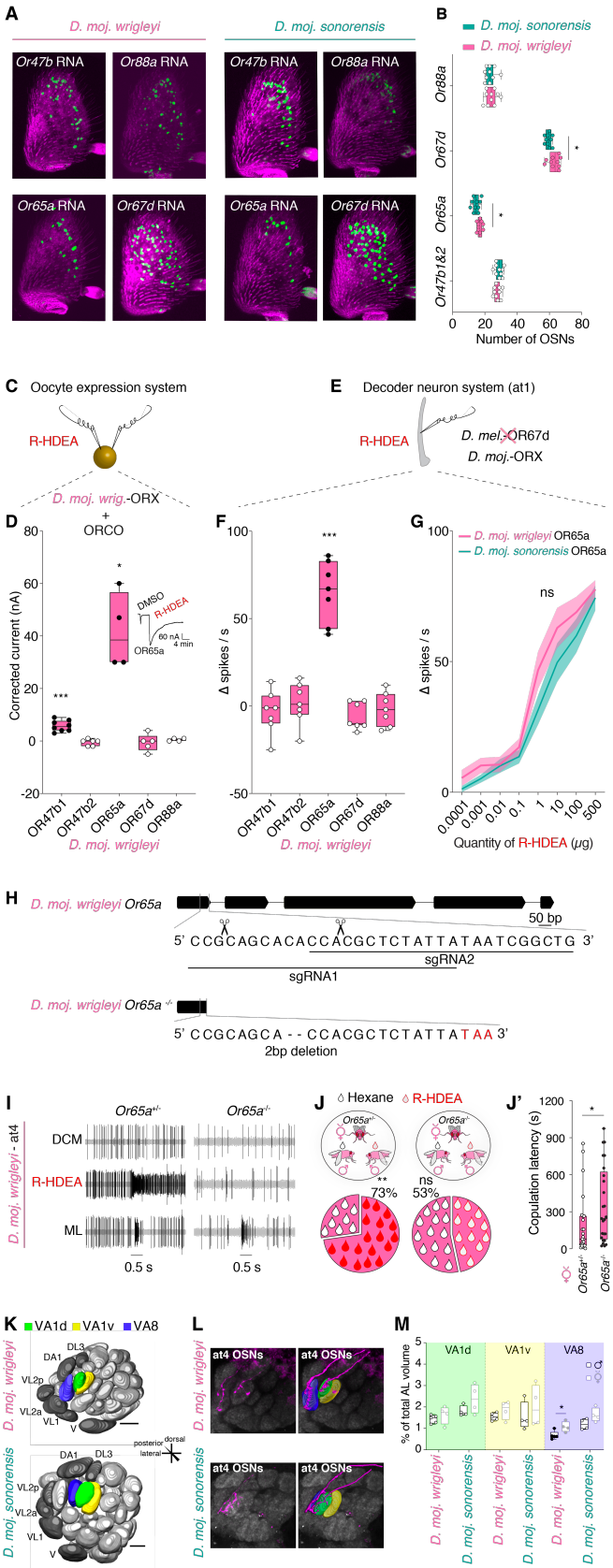

1135
1136

Fig. 6

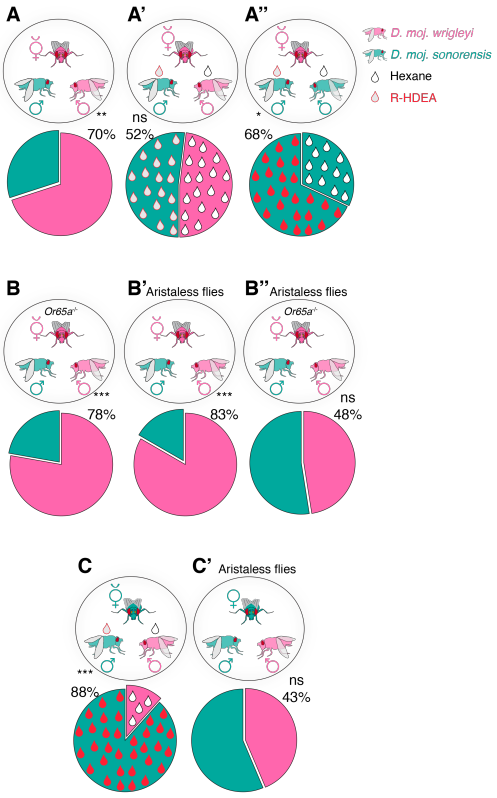

1137
1138

Supplementary Materials for

Mate discrimination among subspecies through a conserved olfactory pathway

Mohammed A. Khallaf, Thomas O. Auer, Veit Grabe, Ana Depetris-Chauvin, Byrappa Ammagarahalli, Dan-Dan Zhang, Sofía Lavista-Llanos, Filip Kaftan, Jerrit Weißflog, Luciano M. Matzkin, Stephanie M. Rollmann, Christer Löfstedt, Aleš Svatoš, Hany K.M. Dweck, Silke Sachse, Richard Benton, Bill S. Hansson and Markus Knaden

Corresponding author email: mknaden@ice.mpg.de (M.K.)
hansson@ice.mpg.de (B.S.H)

The PDF file includes:

Fig. S1. Sexual behaviors of *D. mojavensis* subspecies.
Fig. S2. Chemical analysis of *D. mojavensis* subspecies.
Fig. S3. OCDA-induce courtship suppression, while the other acetates do not elicit attraction.
Fig. S4. Conserved detection mechanism of R-HDEA.
Fig. S5. Functional characterization of sex pheromone receptors and generation of white mutant flies.
Fig. S6. Characterization of antennal lobe glomeruli in *D. mojavensis* subspecies.
Fig. S7. S-HDEA and HDA are not involved in sexual isolation among *D. mojavensis* subspecies.
Table S1. List of Drosophila socks, chemicals, oligonucleotides, and software used in the study.
Legends for Movies S1 to S9.
Legends for data files S1.
Chemical identification and synthesis

Other supplementary material for this manuscript includes:

Movie S1. Sexual behaviors of *D. mojavensis wrigleyi*.
Movie S2. Sexual behaviors of *D. moj. mojavensis*.
Movie S3. Sexual behaviors of *D. moj. sonorensis*.
Movie S4. Sexual behaviors of *D. moj. baja*.
Movie S5. 3-D reconstruction of *D. moj. wrigleyi* antennal lobe (female).
Movie S6. 3-D reconstruction of *D. moj. sonorensis* antennal lobe (female).
Movie S7. Neurobiotin backfilled neurons from at4 sensillum in *D. moj. wrigleyi*.
Movie S8. Neurobiotin backfilled neurons from at4 sensillum in *D. moj. sonorensis*.
Movie S9. Neurobiotin backfilled neurons from at1 sensillum in *D. moj. wrigleyi*.
Data file S1. Sequence alignments of *Or47b1* and *Or47b2* loci in *D. moj. wrigleyi* (provided as Fasta file).

Fig. S1

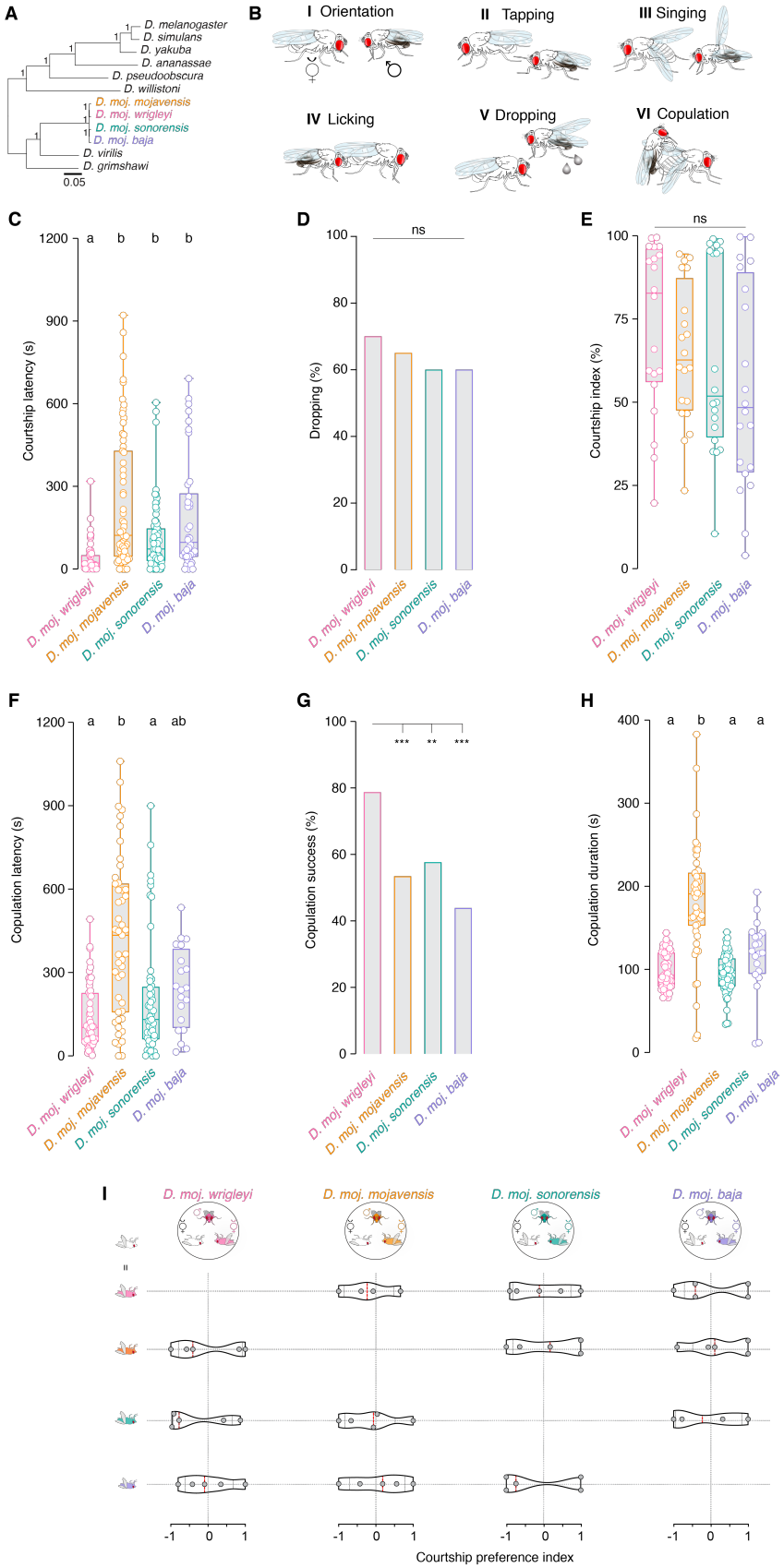

Fig. S1. Sexual behaviors of *D. mojavensis* subspecies.

(A) Phylogenetic relationship among the four *D. mojavensis* subspecies and other *Drosophila* species using the recent genomic analysis of *D. mojavensis* (*22*) and the *D. virilis, D. grimshawi, D. willistoni, D. pseudoobscura, D. ananassae, D. yakuba, D. simulans*, and *D. melanogaster* FlyBase assemblies

(FB2019_04) based on concatenated sequences of 2177 loci. Scale bar for branch length represents the number of substitutions per site. Bootstrap values are indicated by the numbers at the nodes.
(B) Schematic drawing of courtship behaviors of the four *D. mojavensis* subspecies. (**I**) orientation, (**II**) tapping with forelegs, (**III**) singing by wing fanning, (**IV**) licking the female genitals, (**V**) anal droplet discharge, and (**VI**) copulation attempt.
(C) Courtship latency of males toward virgin con-subspecific females in seconds (s) within a 20-minute time window. During the first minute, most males were eager to court by orienting and following the females. Among the four subspecies, *D. moj. wrigleyi* males exhibited shorter and less variable latencies to court. In this and the below panels, age of males and females is 10 days. Boxplots show the median, first and third quartile of the data. Different letters indicate significant differences between subspecies, Kruskal-Wallis test with Dunn's post-hoc correction (*n* from left to right = 60, 63, 74, and 38 replicates).
(D) Percentage of males that released a fluidic droplet from their anus while courting the female. This panel reveals that more than half of the tested males while courting the female released a fluidic droplet from their anus. See fig. S2G for chemical analysis of these droplets. Courtship behaviors were recorded by GoPro Camera (Watch movies S1 to 4 for details). Ns, Fisher's exact test (*n* = 10-20 per subspecies).
(E) Courtship index [%] that males reveal toward their virgin con-subspecific females. In response to the rapid male courtship elements, females slow down their movement, quiver their abdomen, vibrate their wings, and scissor them as signs for acceptance, while kicking with legs or accelerating the movement speed to signal rejection (Watch movies S1 to 4). Overall, courtship rituals were comparable among the four subspecies. Ns $P > 0.05$, Kruskal-Wallis test with Dunn's post-hoc correction (*n* =20).
(F) Copulation latency in seconds (s). Males exhibiting no courtship behavior were excluded from analysis. *D. moj. wrigleyi* males exhibited shorter and less variable latencies to copulate. Kruskal-Wallis test with Dunn's post-hoc correction (*n* from left to right (the number of successful copulations in fig. 1SB) = 52, 47, 53, and 20).
(G) Copulation success [%] of virgin couples in the different *D. mojavensis* subspecies within a 20-minute time window. Among the four subspecies, *D. moj. wrigleyi* males exhibited a higher percentage to be accepted for copulation. Fisher's exact test (*n* (from left to right) = 60, 63, 74, and 38 replicates).
(H) Copulation duration of *D. mojavensis* subspecies in seconds (s). Unlike the prolonged copulation time in *D. melanogaster* (≥ 15 min) (*58*), copulation lasts for ~2-3 min in the *D. mojavensis* subspecies. Kruskal-Wallis test with Dunn's post-hoc correction (*n* from left to right (the number of successful copulations in fig. 1SB) = 52, 47, 53, and 20).
(I) Top row: Competition mating arenas where a male of each *D. mojavensis* subspecies had the choice to court with con-subspecific female or a female of one of the other three subspecies (both are freeze-killed virgin females) (color coded as in Fig. 1A). Below: Violin plots represent the courtship preference indices of males between females (*n* = 4-5 replicates), Ns $P > 0.05$, Wilcoxon signed rank test pairs to zero.

Fig. S2

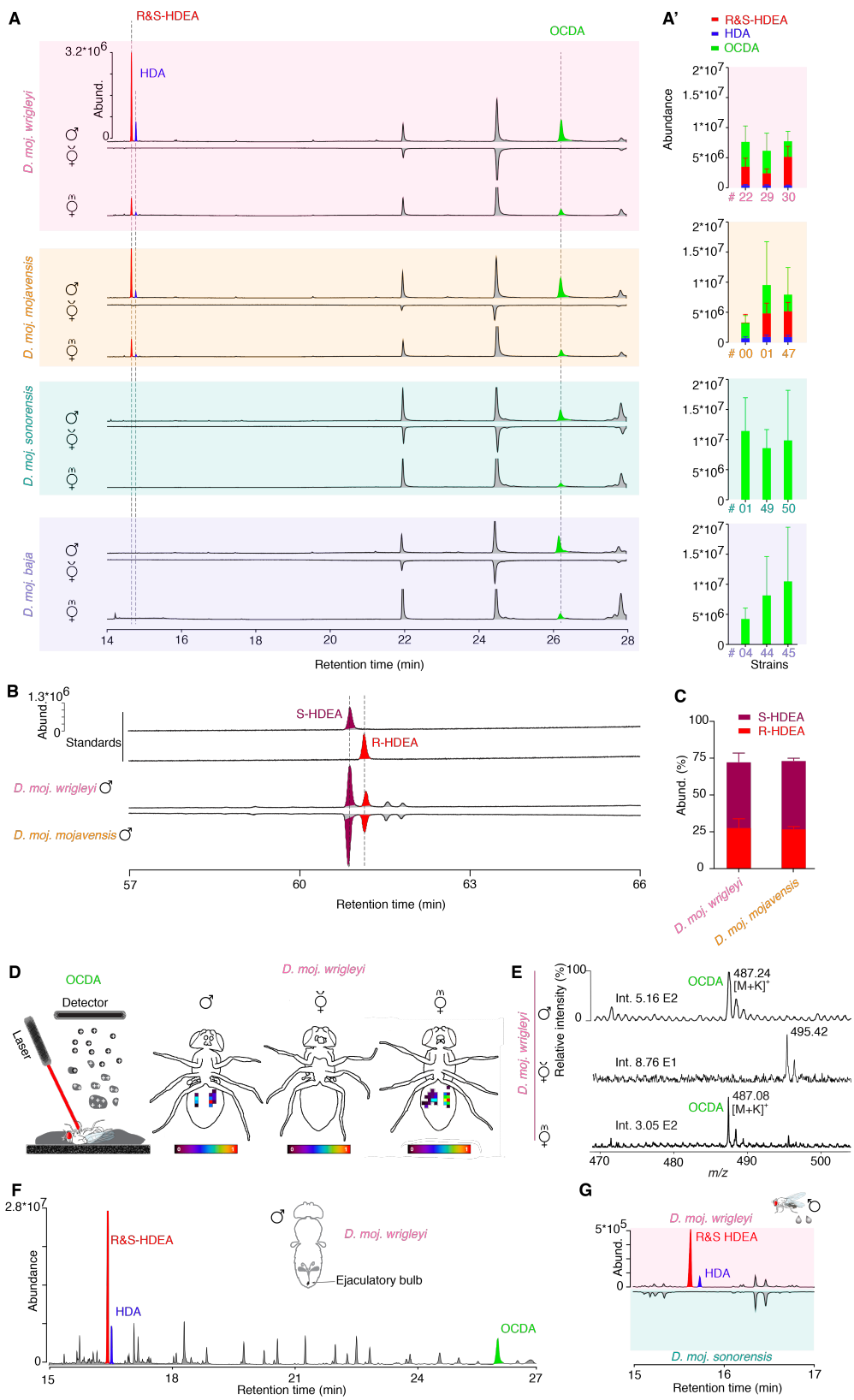

Fig. S2. Chemical analysis of *D. mojavensis* subspecies.
(A) Representative gas chromatograms of hexane-body wash of 10-day-old male (virgin) and female flies (virgin and mated) (n = 5). Colored peaks are the male-transferred compounds during mating; red, R/S–HDEA; blue, HDA; light green, OCDA.

(**A'**) Amount of the male-specific compounds in three different strains per each subspecies (*D. moj. wrigleyi*: 15081-1352.22, 15081-1352.29, and 15081-1352.30; *D. moj. mojavensis*: 15081-1352.47, 15081-1352.00, and 15081-1352.01; *D. moj. sonorensis:* 15081-1351.01, 15081-1352.49, and 15081-1352.50; *D. moj. baja*: 15081-1351.04, 15081-1352.44, and 15081-1352.45. Colored bars and error bars indicate mean abundances and SEM of the three male-specific acetates (n = 3-4 males per subspecies).

(B) Extracted ion chromatogram of hexane body wash of 10-day-old virgin male at the qualifier ion *m/z* 236 processed by chiral column (n = 3). Colored peaks are S (brown) and R (red) enantiomers of 10*Z*-heptadecen-2yl acetate.

(C) Amount percentage of R and S-HDEA enantiomers in *D. moj. wrigleyi* and *D. moj. mojavensis*. Ns $P > 0.01$, Mann Whitney U test (n = 3).

(D) Representative imaging mass spectrometry for OCDA (see Materials and Methods for details) by MALDI-TOF technique (Left: schematic drawing) of the abdominal surfaces of a 10-day-old male (virgin) and female fly (virgin and mated) (n = 3).

(E) Representative MALDI-TOF mass spectra of male (virgin) and female flies (virgin and mated) at the qualifier ion *m/z* 487 [M+K]+ of OCDA.

(F) Representative gas chromatogram of ejaculatory bulbs of *D. moj. wrigleyi* obtained by solvent-free TD-GC-MS (Top: schematic drawing) of 10-day-old males (virgin) (n = 3 replicates, each contains 5 ejaculatory bulbs). TD-GC-MS analyses reveal that all three acetates are present in high amounts in the ejaculatory bulb. Colored peaks indicate the male-specific compounds.

(G) Gas chromatograms of male-released droplets during courtship in *D. moj. wrigleyi and D. moj. sonorensis* (n = 3). Chemical analysis revealed the presence of R/S-HDEA and HDA in *D. moj. wrigleyi* droplets but not in droplets of *D. moj. sonorensis*, while OCDA was absent in the droplets of both subspecies. Due to the absence of OCDA signal, the x-axis was shortened. Colored peaks indicate the male-specific acetates (R/S-HDEA and HDA).

Fig. S3

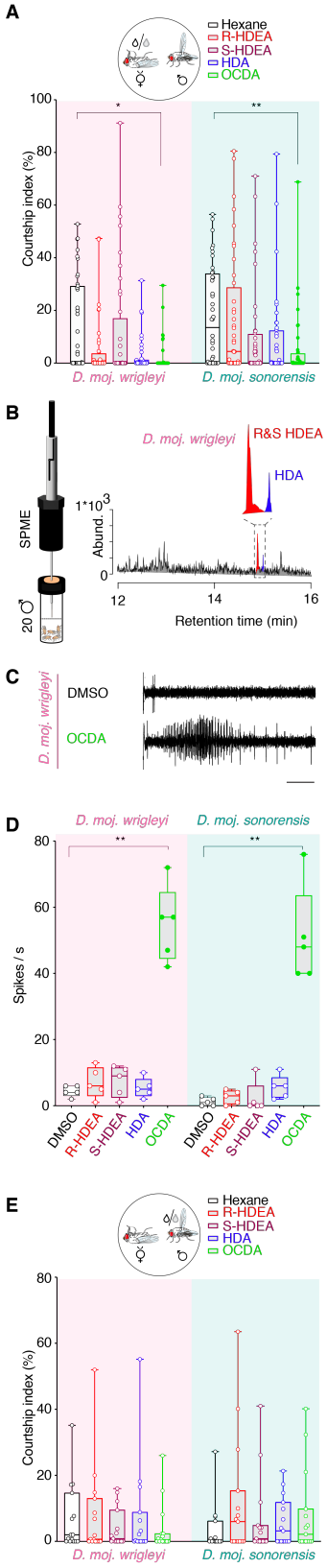

Fig. S3. OCDA-induce courtship suppression.

(A) Courtship index [%] of males towards dead con-subspecific females perfumed with hexane as a control (black) or one of the male-specific acetates diluted in hexane (colored). Kruskal-Wallis test with Dunn's post-hoc correction. Ns P > 0.05; * P < 0.05; ** P < 0.01 (*n* = 40 assays).

(B) Headspace collection by SPME (see schematic drawing) and corresponding representative gas chromatogram from 10-day-old males of *D. moj. wrigleyi* trapped inside a mesh (dashed line) in a vial. Enlarged window represents R&S-HDEA (red) and HDA (blue) (n = 3 replicates, each contains 20 males). Due to the absence of OCDA signal, the x-axis was shortened.
(C) Representative tip recording traces from foreleg-tarsi using DMSO or OCDA (1 µg diluted in DMSO). Scale bar represents 150 milliseconds (ms).
(D) Tip recording measurements from foreleg-tarsi of *D. moj. wrigleyi* and *D. moj. sonorensis* using R or S-HDEA, HDA, OCDA. Ns $P > 0.05$; ** $P < 0.01$, Kruskal-Wallis test followed by Dunn's multiple comparisons test (n = 5).
(E) Top: Schematic of courtship arena where a dead virgin female (left, *D. moj. wrigleyi*; right, *D. moj. sonorensis*) is courted by a con-subspecific male perfumed with hexane or one of the other acetates. Below, y-axis represents courtship index [%] (equal the time a male exhibits courtship behaviors (fig. S1B) / total amount of recording time (10 min)). Ns > 0.05, Kruskal-Wallis test followed by Dunn's multiple comparisons test (n = 15). Males and females used in this and other panels are 10 days old.

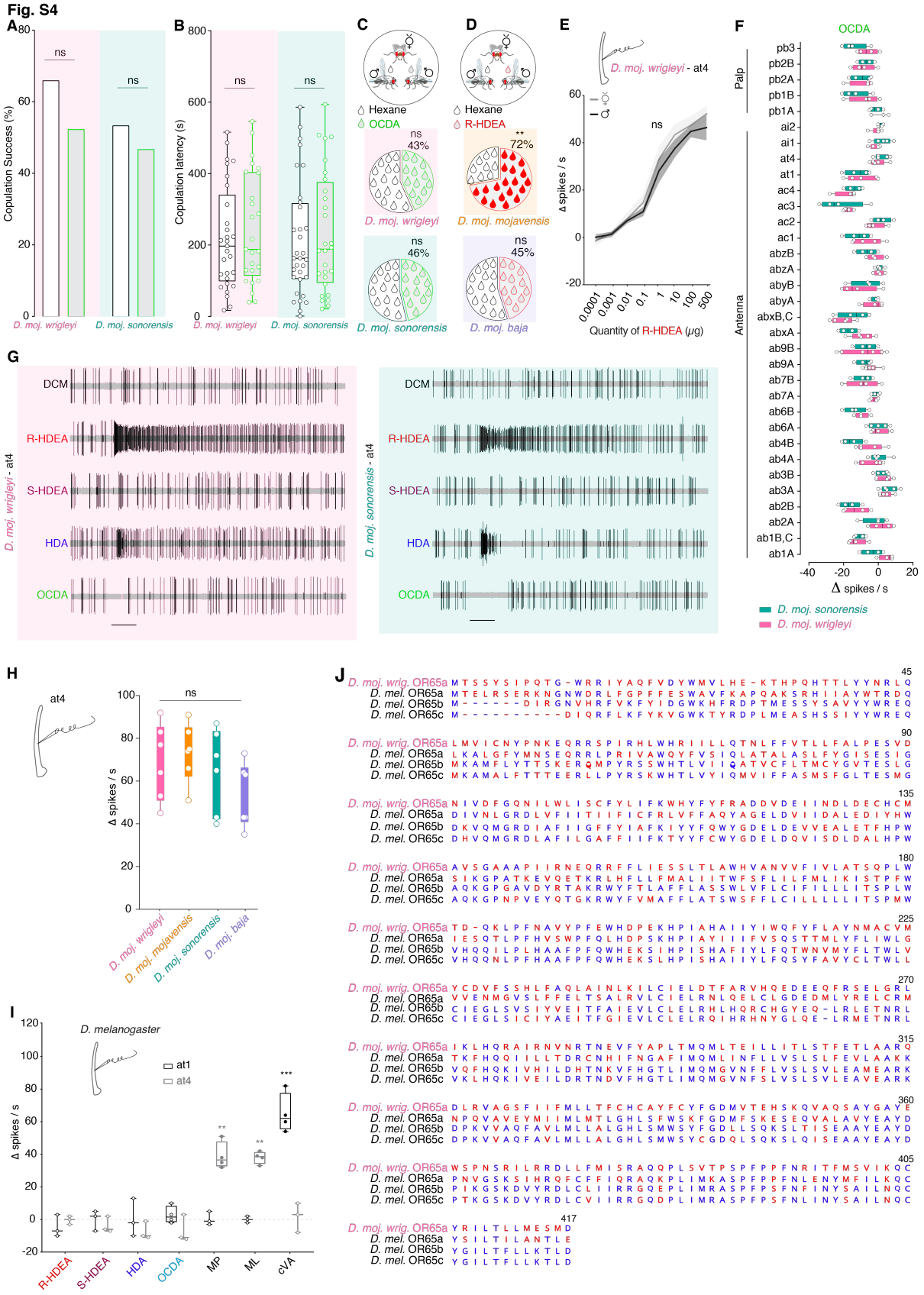

Fig. S4. Conserved detection mechanism of R-HDEA

(A) Copulation success [%] of *D. moj. wrigleyi* and *D. moj. sonorensis* males perfumed with hexane or OCDA diluted in hexane. See Fig. 4A for details (n = 40).

(B) Copulation latency of the same males perfumed with hexane or OCDA diluted in hexane. See Fig. 4B for details. (*n* from left to right = 29, 25, 32, and 28).
(C) Competition between two con-subspecific males, perfumed with OCDA or with hexane. See Fig. 4C for details. Ns $P > 0.05$, chi-square test (*n* from top to bottom = 120 and 112).
(D) Top: competition between two males of *D. moj. mojavensis*, to mate with a virgin female. *** $P < 0.001$, chi-square test. Bottom: competition between two males of *D. moj. baja*, perfumed with R-HDEA or hexane, to copulate with a virgin con-subspecific female. Ns $P > 0.05$, chi-square test (*n* from top to bottom = 100 and 116).
(E) Dose-response relationships for at4 neurons of *D. moj. wrigleyi* females (light grey) and males (dark grey) toward R-HDEA (Mean ± SEM). Two-way ANOVA followed by Sidek's multiple comparison test between the two sexes responses to the same stimulus, ns $P > 0.05$ (*n* = 5 per single dose).
(F) Single-sensillum recording (SSR) measurements from all types of olfactory sensilla on antenna and maxillary palp, with OCDA (10 µg) as a stimulus. ab, antennal basiconic sensilla; ac, antennal coeloconic; at, antennal trichoid; ai, antennal intermediate; pb, palp basiconic (*n* = 3-6).
(G) Representative SSR traces from at4 sensillum of *D. moj. wrigleyi* and *D. moj. sonorensis* to DCM (as solvent), R-HDEA, S-HDEA, HDA, and OCDA (100 µg). Scale bar represents stimulus duration (0.5 second).
(H) Responses of at4 sensilla in *D. mojavensis* subspecies (color coded as in Fig. 1A) to R-HDEA (1000 µg). Ns $P > 0.01$, Kruskal-Wallis test between different treatments with Dunn's post-hoc correction. (*n* = 6).
(I) Responses of *D. melanogaster* at1 (black) and at4 (grey) to R, HDEA, S-HDEA, HDA, OCDA, methyl palmitate (MP; diagnostic odor for Or88a), methyl laurate (ML; diagnostic odor for Or47b and Or88a) and *c*VA (diagnostic odor for Or67d neurons) (10 µg diluted in DCM). SSR analyses reveal that none of the *D. moj. wrigleyi* male-specific acetates elicited any response in the at1 nor at4 sensillum of *D. melanogaster*. Filled circles in this panel indicate significant difference from solvent responses. Ns $P > 0.05$; ** $P < 0.01$; *** $P < 0.001$, Mann Whitney U test (*n* = 3-4).
(J) Alignments of *D. moj. wrigleyi*-OR65a and *D. melanogaster*-OR65a/b/c protein sequences. Blue letters represent the similarities while red letters represent the polymorphic sites.

Fig. S5

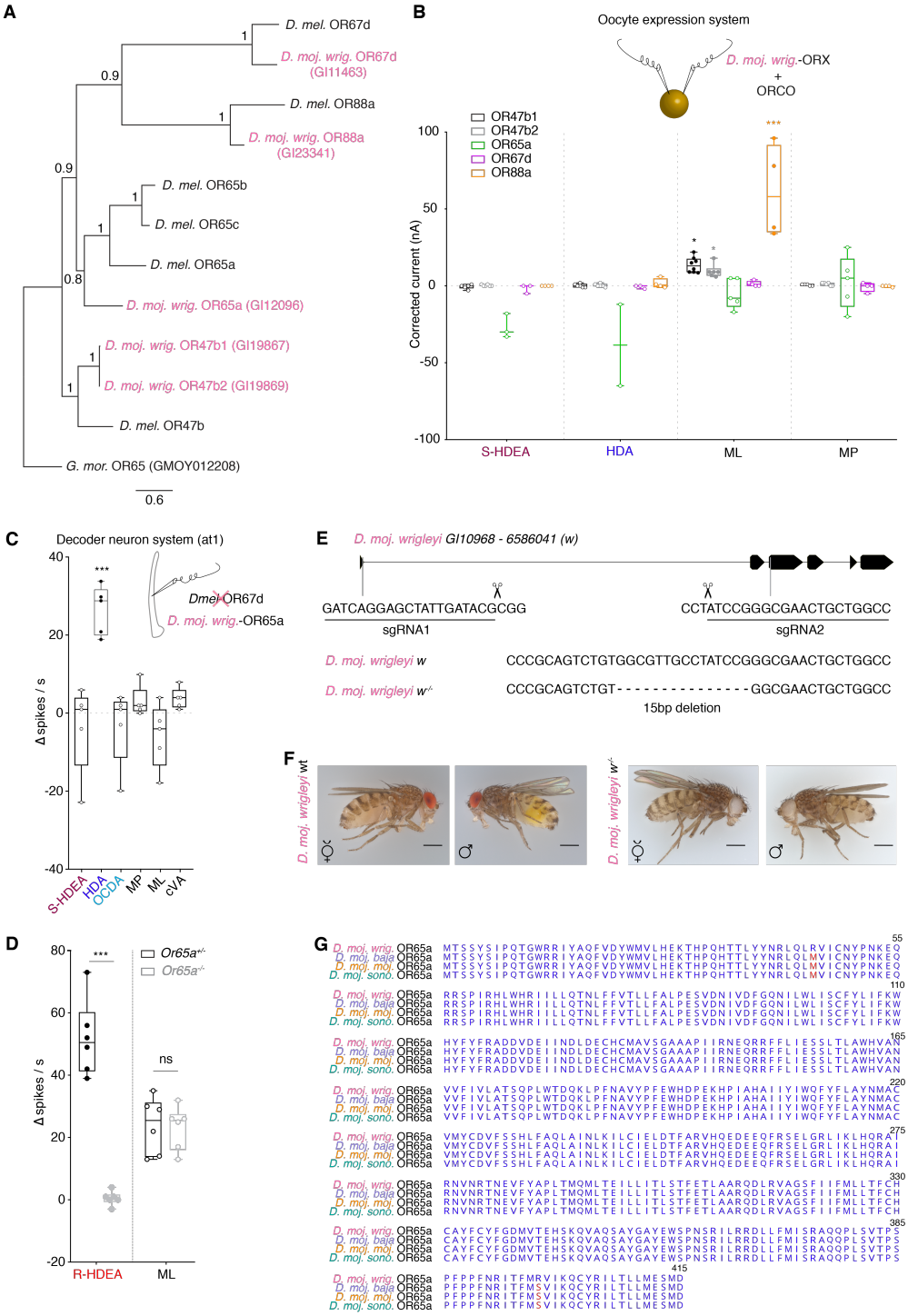

Fig. S5. Functional characterization of sex pheromone receptors and generation of white mutant flies.

(A) Phylogenetic analysis of pheromone receptors (OR67d, OR88a, Or65 and OR47b) in *D. melanogaster* and *D. moj. wrigleyi* using Or65a ortholog in *Glossina morsitans* as an outgroup. Of the

six pheromone sensing receptors in *D. melanogaster*, five are present in the *D. moj. wrigleyi* genome (*11*): GI19867 and GI19869 (OR47b1 and OR47b2, respectively), GI12096 (OR65a/b/c), GI11463 (OR67d), and GI23341 (OR88a). GI12096 has three paralogs in *D. melanogaster* (OR65a/b/c) and shares the highest degree of protein alignment with *D. melnaogaster*-OR65a (*11*) compared to others (fig. S4J). The scale bar for branch length represents the number of substitutions per site. Bootstrap values are indicated by the numbers at the nodes.

(B) Responses of the five odorant receptors (indicated in different colors), heterologously expressed in *X. laevis* oocytes to S-HDEA, HDA, methyl laurate (diagnostic odor for OR47b), and methyl palmitate (diagnostic odor for OR88a) (1mM diluted in DMSO). Filled circles in this and fig. S5C indicate significant difference from solvent responses, ns $P > 0.05$; * $P < 0.05$; *** $P < 0.001$, Mann Whitney U test (n = 2-8).

(C) Responses of the *D. moj. wrigleyi-Or65*a gene heterologously expressed in *D. melanogaster* at1 to previous-mentioned compounds and cis-vaccenyl acetate (diagnostic odor for Or67d) (10 µg diluted in DCM). Ns $P > 0.05$; *** $P < 0.001$, Mann Whitney U test (n = 3-4).

(D) Responses of *Or65a* heterozygous (black) and homozygous (grey) animals to R-HDEA and methyl laurate (ML) (100 µg diluted in DCM). Filled-circles indicate significant difference between both groups. Ns $P > 0.05$; *** $P < 0.001$, Mann Whitney U test (n = 6).

(E) Schematic drawing of the structure of the *white* gene (*GI 10968-6586041*) illustrating the strategy for generating knockouts using CRISPR/Cas9. The two guide RNA sequences are shown below; scissors denote the cutting sites. All knock-outs were validated by sequencing the targeted locus in homozygous mutants prior to establishing lines. The *white* gene knockout animals carry a 15 bp deletion.

(F) A macrograph of a lateral view of wildtype and *white* mutant female (right) or wildtype and *white* mutant male (left) of *D. moj. wrigleyi*. In addition to the eye color change, the yellowish color of the male's accessory glands disappeared. Scale bar represents 500 µm.

(G) Protein alignment of OR65a in the four *D. moj.* subspecies in an open reading frame. Blue letters represent the similarities while red letters represent the polymorphic sites.

Fig. S6

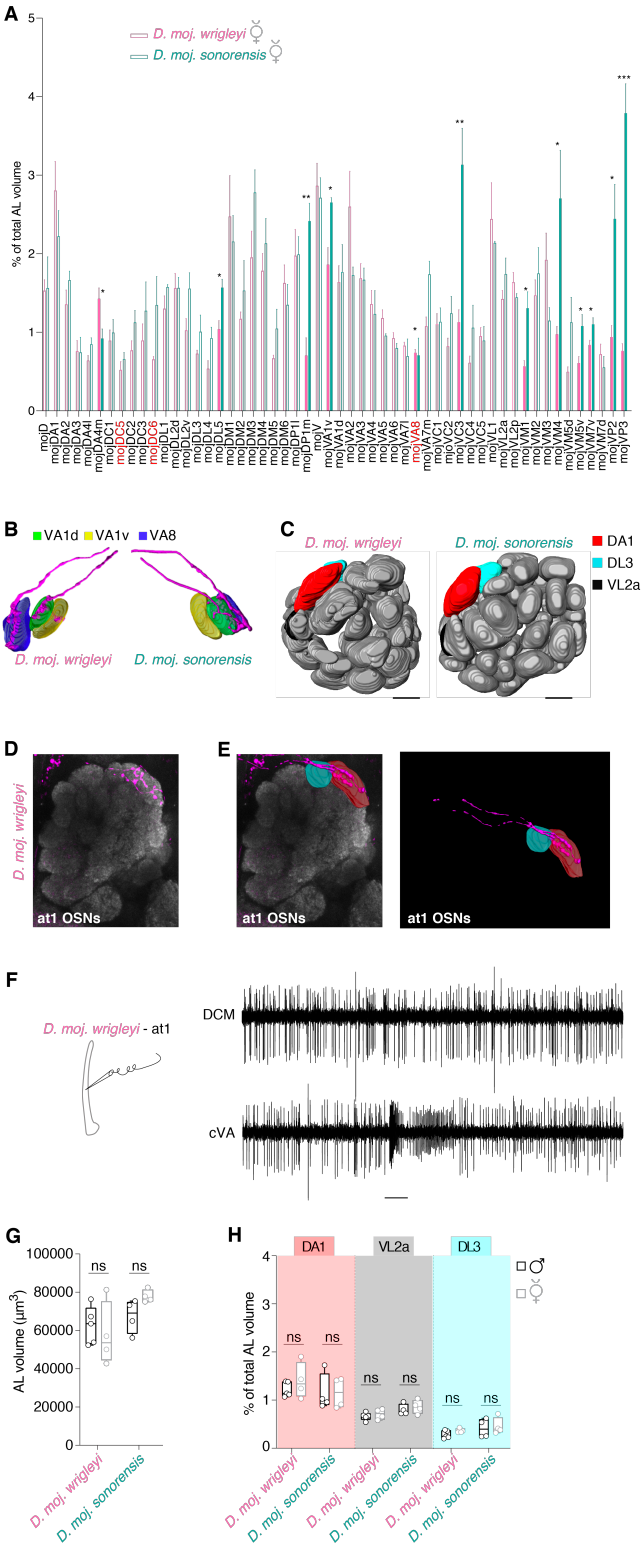

Fig. S6. Characterization of antennal lobe glomeruli in *D. mojavensis* subspecies.
(A) Normalized volumes of 54 glomeruli (out of 57; other three glomeruli could be identified but not accessed for volumetric analysis) for *D. moj. wrigleyi* and *D. moj. sonorensis* females. Glomeruli in red are *D. mojavensis*-specific novel glomeruli, which named according to their relative position to the

adjacent glomeruli. Landmark glomeruli (See Materials and Methods) were used as to compare antennal lobes of *D. mojavensis* and *D. melanogaster* as previously used in (*54*). However, future molecular markers will be necessary to verify this identification. Filled bars indicate significant differences between both subspecies. All data passed Shapiro–Wilk normality test, except the data of DM2, V, and VA2. Normally-distributed data are analyzed by Unpaired t test, otherwise Mann Whitney U test is used. ns $P > 0.05$; * $P < 0.05$; ** $P < 0.01$; *** $P < 0.001$ (n = 3-4 animals per subspecies). See fig. S6A for more details.

(B) A pattern of neurobiotin backfilled neurons (magenta) from at4 sensillum that reveals similar innervation in *D. moj. wrigleyi* (right) and *D. moj. sonorensis* (left) to VA8, VA1v and VA1d glomeruli.

(C) Three-dimensional reconstruction of antennal lobes from representative female brains of *D. moj. wrigleyi, D. moj. sonorensis* and *D. melanogaster*. DA1, red; DL3, cyan; VL2a, black. Scale bar represents 12 µm.

(D) Fluorescent staining for neurobiotin (green) and nc82 (magenta) in *D. moj. wrigleyi* antennal lobe backfilled from at1 sensillum (identified by electrophysiological recordings; Fig. 4E). Backfilling of the at1 sensillum of *D. moj. wrigleyi* revealed a similar innervation target as in *D. melanogaster* (*17*) to the DA1 glomerulus but with two neuronal tracts innervating separately the anterior and posterior regions of this glomerulus. The backfill image corresponds to a projection of 28 Z-stacks (Watch movie S9).

(E) Reconstructions for the backfill signal that innervate the DA1 (red) but not DL3 (cyan) glomerulus.

(F) Representative SSR traces from at1 sensillum of *D. moj. wrigleyi* DCM, *cis*-vaccenyl acetate (cVA, 100 µg). Consistent with the innervation pattern of *D. mojavensis* at1 neurons, SSR analysis of the at1 sensillum revealed the presence of at least two OSNs in this sensillum type (*59*). Scale bar represents the stimulus duration (0.5 s).

(G) Antennal lobe volumes (μm^3) for males (black) and females (grey) of *D. moj. wrigleyi* and *D. moj. sonorensis*. Filled circles in this and below panels indicate significant difference from the other sex within the same species, ns $P > 0.05$; * $P < 0.05$; ** $P < 0.01$, Mann Whitney U test (n = 4-6).

(H) Normalized volumes of DA1, VL2a and DL3 for *D. moj. wrigleyi* and *D. moj. sonorensis* females and males.

Fig. S7

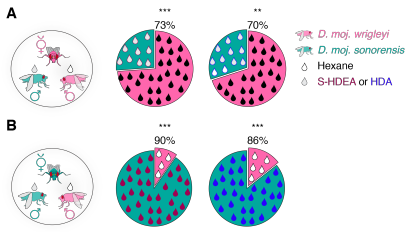

Fig. S7. S-HDEA and HDA are not involved in sexual isolation among *D. mojavensis* subspecies. **(A)** Competition between two males of different subspecies, *D. moj. sonorensis* male perfumed with S-HDEA (red droplet, left panel) or HDA (blue droplet, right panel) and *D. moj. wrigleyi* male perfumed with hexane (black droplets), to copulate with *D. moj. wrigleyi* virgin female. Pie-charts in A-B represent copulation success [%] of the rival males, ** $P < 0.01$; *** $P < 0.001$, chi-square test (n from left to right = 92 and 80, respectively). All males and females used in this and other panels were 10-day-old virgin flies.

(B) Competition between two males of different subspecies, *D. moj. sonorensis* male perfumed with S-HDEA (red droplet, left panel) or HDA (blue droplet, right panel) and *D. moj. wrigleyi* male perfumed with hexane (black droplets), to copulate with *D. moj. sonorensis* virgin female. (n from left to right = 84 for both panels).

1561

1562 **Table S1**

REAGENT or RESOURCE	SOURCE	IDENTIFIER
Experimental Models: Species or strains (*Drosophila*) and Breeding medium		
D. melanogaster, Canton-S strain (Cornmeal food)	NA	NA
D. melanogaster; y w M(eGFP.vas-int.Dm)ZH-2A; M(RFP.attP)ZH-51D; +; + (Cornmeal food)	FlyC31	ΦX-51D
D. melanogaster, y w; Bl/CyO; TM2/TM6B (Cornmeal food)	Lindsely and Zimm, 1992	NA
D. melanogaster, w-; Bl/CyO; D.mel-Or67d^{Gal4}/TM6B (Cornmeal food)	Kurtovic, 2007	NA
D. melanogaster, w-; UAS-D.moj.wirg.-Or47b1; D.mel-Or67d^{Gal4} (Cornmeal food)	This paper	NA
D. melanogaster, w-; UAS-D.moj.wirg.-Or47b2; D.mel-Or67d^{Gal4} (Cornmeal food)	This paper	NA
D. melanogaster, w-; UAS-D.moj.wirg.-Or65a; D.mel-Or67d^{Gal4} (Cornmeal food)	This paper	NA
D. melanogaster, w-; UAS-D.moj.wirg.-Or67d; D.mel-Or67d^{Gal4} (Cornmeal food)	This paper	NA
D. melanogaster, w-; UAS-D.moj.wirg.-Or88a; D.mel-Or67d^{Gal4} (Cornmeal food)	This paper	NA
D. melanogaster, w-; UAS-D.moj.sono.-Or65a; D.mel-Or67d^{Gal4} (Cornmeal food)	This paper	NA
D. mojavensis wrigleyi (Banana food)	NDSSC	15081-1352.22
D. mojavensis wrigleyi (Banana food)	NDSSC	15081-1352.29
D. mojavensis wrigleyi (Banana food)	NDSSC	15081-1352.30
D. mojavensis baja (Banana food)	NDSSC	15081-1351.04
D. mojavensis baja (Banana food)	NDSSC	15081-1352.44
D. mojavensis baja (Banana food)	NDSSC	15081-1352.45
D. mojavensis mojavensis (Banana food)	NDSSC	15081-1352.47
D. mojavensis mojavensis (Banana food)	NDSSC	15081-1352.00
D. mojavensis mojavensis (Banana food)	NDSSC	15081-1352.01
D. mojavensis sonorensis (Banana food)	NDSSC	15081-1351.01
D. mojavensis sonorensis (Banana food)	NDSSC	15081-1352.49
D. mojavensis sonorensis (Banana food)	NDSSC	15081-1352.50
D. moj. wrigleyi Or65a$^{-/-}$ (Banana food)	This paper	NA
D. moj. wrigleyi w$^{-/-}$ (Banana food)	This paper	NA
Chemicals and their Diagnostic Uses		
Isopropyl benzoate (ab1A, ab2B)	Sigma-Aldrich	94-46-2

Dimethyl disulfide (ab1B)	Sigma-Aldrich	624-92-0
Hexyl acetate (ab3A, ab7A)	Sigma-Aldrich	142-92-7
Isopentyl acetate (ab4A)	Sigma-Aldrich	123-92-2
Geosmin (ab4B)	Sigma-Aldrich	16423-19-1
Guaiacol (ab6B)	Sigma-Aldrich	90-05-1
Ethyl lactate (ab7B)	Sigma-Aldrich	97-64-3
Acetophenone (ab9B)	Sigma-Aldrich	98-86-2
1-hexanol (abzB)	Merck	111-27-3
Ethyl 3-hydroxybutyrate (abxB)	Fluka	5405-41-4
4-ethylguaiacol (pb1B)	Sigma-Aldrich	2785-89-9
(-)-fenchone (pb2A)	Sigma-Aldrich	7787-20-4
2-heptanone (pb3B)	Sigma-Aldrich	110-43-0
Ammonia (ac1)	Sigma-Aldrich	7664-41-7
1,4-Diaminobutane (ac2)	Sigma-Aldrich	110-60-1
1-octanol (ac3)	Sigma-Aldrich	111-87-5
Phenylacetaldehyde (ac4)	Sigma-Aldrich	122-78-1
Farnesol (ai1)	Sigma-Aldrich	4602-84-0
Valencene (ai2)	Sigma-Aldrich	4630-07-3
cis-vaccenyl acetate (at1 and Oocyte experiments)	Biomol	6186-98-7
Methyl laurate (at4 and Oocyte experiments)	Fluka	111-82-0
Methyl palmitate (at4 and Oocyte experiments)	Sigma-Aldrich	112-39-0
Dichloromethane (DCM, Solvent for SSR experiments)	Sigma-Aldrich	75-09-2
Hexane (Hex, Solvent for Behavioral experiments)	Sigma-Aldrich	110-54-3
Dimethyl sulfoxide (DMSO, Solvent for Oocyte experiments)	Sigma-Aldrich	200-664-3
(*R*,*Z*)-10-Heptadecen-2-ylacetate (R-HDEA)	This paper	NA
(*S*,*Z*)-10-Heptadecen-2-ylacetate (S-HDEA)	This paper	NA
Heptadec-2-yl acetate (HDA)	This paper	NA
(19*Z*,22*Z*)- Octacosadienyl acetate (OCDA)	This paper	NA
Oligonucleotides and their targets (BamHI site, Kozaq sequence, and XbaI site)		
Orco Fwd, (to amplify from cDNA) ATGGCTACATCAATGCAGCCCGGCAAG	This paper	NA
Orco Rev, (to amplify from cDNA) TCACTTGAGTTGCACCAGCAC	This paper	NA
Orco Fwd, (to clone in pCS2+ vector) CGCGGATCCGCCACCATGGCTACATCAATGCAGCCCGGCAAG	This paper	NA
Orco Rev, (to clone in pCS2+ vector) GCTCTAGATCACTTGAGTTGCACCAGCAC	This paper	NA
Or47b Fwd, (to amplify from cDNA) ATGGCCAATGGGGATTTCAAG	This paper	NA
Or47b Rev, (to amplify from cDNA) TTACATGGCCTCACGCAGCA	This paper	NA

Or47b Fwd, (to clone in pCS2+ vector) CGCGGATCCGCCACCATGGCCAATGGGGATTTCAAG	This paper	NA
Or47b Rev, (to clone in pCS2+ vector) GCTCTAGATTACATGGCCTCACGCAGCA	This paper	NA
Or65a Fwd, (to amplify from cDNA) ATGACGAGCAGCTATAGTATAC	This paper	NA
Or65a Rev, (to amplify from cDNA) TTAATCCATGCTCTCCATCAAG	This paper	NA
Or65a Fwd, (to clone in pCS2+ vector) CGCGGATCCGCCACCATGACGAGCAGCTATAGTATAC	This paper	NA
Or65a Rev, (to clone in pCS2+ vector) GCTCTAGATTAATCCATGCTCTCCATCAAG	This paper	NA
Or67d Fwd, (to amplify from cDNA) ATGGCGAAGACGGCTGTG	This paper	NA
Or67d Rev, (to amplify from cDNA) TTATATCTCGTAGTCCAAGTACGTAATCATC	This paper	NA
Or67d Fwd, (to clone in pCS2+ vector) CGCGGATCCGCCACCATGGCGAAGACGGCTGTG	This paper	NA
Or67d Rev, (to clone in pCS2+ vector) GCTCTAGATTATATCTCGTAGTCCAAGTACGTAATCATC	This paper	NA
Or88a Fwd, (to amplify from cDNA) ATGGATAACATAAATCAACCCA	This paper	NA
Or88a Rev, (to amplify from cDNA) CTATTGTCGTGACTTGAGAAATGTG	This paper	NA
Or88a Fwd, (to clone in pCS2+ vector) CGCGGATCCGCCACCATGGATAACATAAATCAACCCA	This paper	NA
Or88a Rev, (to clone in pCS2+ vector) GCTCTAGACTATTGTCGTGACTTGAGAAATGTG	This paper	NA
Guide sequence 1 for *D. moj. white* (*w* sgRNA1), GGCCAGCAGTTCGCCCGGAT	This paper	NA
Or47b Fwd (to amplify RNA *in situ* probe), ATCGCGATTTGCCCTACCAT	This paper	NA
Or47b Rev (to amplify RNA *in situ* probe), AGCTCTTACATGGCCTCACG	This paper	NA
Or65a Fwd (to amplify RNA *in situ* probe), TGGACTACTGGATGGTGCTG	This paper	NA
Or65a Rev (to amplify RNA *in situ* probe), TTAATCCATGCTCTCCATCAAG	This paper	NA
Or67d Fwd (to amplify RNA *in situ* probe), ATGGCGAAGACGGCTGTG	This paper	NA
Or67d Rev (to amplify RNA *in situ* probe), TTATATCTCGTAGTCCAAGTACGTAATCATC	This paper	NA
Or88a Fwd (to amplify RNA *in situ* probe), GTATTGTCAACAGATCGG	This paper	NA
Or88a Rev (to amplify RNA *in situ* probe), TCGCATAGCACATTGATC	This paper	NA
Guide sequence 2 for *D. moj. white* (*w* sgRNA2), GATCAGGAGCTATTGATACG	This paper	NA
w sgRNA1 genotyping Fwd, CGAGCCAATGAACAGATCGTCCT	This paper	NA
w sgRNA1 genotyping Rev, GAACTATGGCACGCTGAGTCCTT	This paper	NA

w sgRNA2 genotyping Fwd, CGGTTTCTAGGCATGTCAATACAC	This paper	NA
w sgRNA2 genotyping Rev, GCCTTGCTCCATAAGTAAATAGCT	This paper	NA
Guide sequence 1 for *D. moj. Or65a* (*Or65a* sgRNA1), CAGCACACCACGCTCTATTA	This paper	NA
Guide sequence 2 for *D. moj. Or65a* (*Or65a* sgRNA2), CGCTCTATTATAATCGGCTG	This paper	NA
Or65a sgRNA1+2 genotyping Fwd, GCGCAATTCGTGGACTACTGGATGG	This paper	NA
Or65a sgRNA1+2 genotyping Rev, GCGCTGCTCCTTGTTCGGATAGTTGC	This paper	NA
Software		
Noldus	Noldus	https://www.noldus.com
ChemStation (F.1.3.2357)	Agilent	https://www.agilent.com
NIST Mass spectra Search Program (v2.2)	NIST	https://www.nist.gov/
ChemDraw Professional (v17.1)	Chem Office 2017	https://www.perkinelmer.com
MassLynx (v4.0)	Waters	https://www.waters.com
BioMap	MS Imaging	https://ms-imaging.org
Geneious (11.0.5)	Geneious	https://www.geneious.com
ImageJ (Fiji)	NIH	https://imagej.net/Fiji
Zen (2)	Zeiss	https://www.zeiss.com
NIS Elements Viewer (v4.5)	Nikon	https://www.nikon.com
AMIRA (v5.6.0)	Visualization Sciences Group	http://www.vsg3d.com
AutoSpike (v3.7)	Synteck	http://www.ockenfels-syntech.com
Cellworks	npielectronic	http://www.npielectronic.de
Tilde	Bas van Steensel lab	https://tide.deskgen.com
GraphPad Prism (v8.2)	GraphPad	https://www.graphpad.com
Rstudio (v1.1.447)	R Consortium	https://www.r-project.org
Illustrator (v23.1.1)	Adobe	http://www.adobe-students.com

Table S1. List of Drosophila socks, chemicals, oligonucleotides, and software used in the study.

Movie S1. Sexual behaviors of *D. mojavensis wrigleyi*.
During the first minute, most males of the four subspecies were eager to court by orienting and following the females. Subsequently, males tapped the females' bodies with their forelegs, followed by wing spreading and fanning for vibrational song production. Females responded to the males' song by vibrating their wings. Males followed the females by extending their proboscis to lick the females' genitalia and then attempted copulation. Males while courting the female in addition released a fluidic droplet from their anus. We called this novel trait "dropping behavior". In response to the rapid male courtship elements, females slow down their movement, quiver their abdomen, vibrate their wings and scissor them as signs for acceptance, while kicking with legs or accelerating the movement speed to signal rejection.

Movie S2. Sexual behaviors of *D. moj. mojavensis*.

Movie S3. Sexual behaviors of *D. moj. sonorensis*.

Movie S4. Sexual behaviors of *D. moj. baja*.

Movie S5. 3-D reconstruction of *D. moj. wrigleyi* antennal lobe (female).

Movie S6. 3-D reconstruction of *D. moj. sonorensis* antennal lobe (female).

Movie S7. Neurobiotin backfilled neurons from at4 sensillum in *D. moj. wrigleyi*.
Fluorescent staining for neurobiotin (green) and nc82 (magenta) of *D. moj. wrigleyi* antennal lobe, backfilled from at4 sensillum.

Movie S8. Neurobiotin backfilled neurons from at4 sensillum in *D. moj. sonorensis*.
Fluorescent staining for neurobiotin (green) and nc82 (magenta) of *D. moj. sonorensis* antennal lobe, backfilled from at4 sensillum.

Movie S9. Neurobiotin backfilled neurons from at1 sensillum in *D. moj. wrigleyi*.
Fluorescent staining for neurobiotin (green) and nc82 (magenta) of *D. moj. wrigleyi* antennal lobe, backfilled from at1 sensillum.

Data file S1. Sequence alignments of *Or47b1* and *Or47b2* loci in *D. moj. wrigleyi* (provided as Fasta file).

Chemical identification and synthesis

Chemical identification

TDU-GC/EIMS data obtained from virgin males and females show three chromatographic peaks abundant in males. The first one (KI 1998) was the most abundant. Molecular ion peak is not visible, but rather *m/z* 236 is abundant. Accurate mass provided molecular composition $C_{17}H_{32}$. A large EE ion series of 194 (236-C3H6), 180, 166 up to 82 (consecutive losses of CH_2) indicate unsaturation in alicyclic chain. Diagnostic peaks at *m/z* 87 (α-cleavage, $C_4H_7O_2$), 61 ($C_2H_3O_2$) 43 indicate acetyl group on position 2. Then *m/z* 236 peak represents $[M\text{-}CH_3COOH]^{+\bullet}$. The double bond position was determined by converting the compound to dimethyldisulfite (DMDS) adduct (*60*). The EIMS spectrum show *m/z* 390 $[M]^{+\bullet}$ and indicative fragments A: *m/z* 245 and *m/z* 185 $[A\text{-}CH_3COOH]^{+}$; B: 145 plus additional ions at *m/z* 87 and 61. Data analysis suggests 10-heptadecen-2-yl-acetate. The prepared (*rac,*10*Z*)-heptadecen-2-yl-acetate (HDEA) show undistinguishable EIMS spectra and chromatographic retention as the natural product. Chirality and enantiomeric purity of natural acetate was determined on a chiral GC column using prepared (*2R,*10*Z*)-heptadecen-2-yl-acetate and (2R*,*10*Z*)-heptadecen-2-yl-acetate standards.

The second peak with longer retention (KI 2017) show in EIMS spectrum low-abundant molecular ion *m/z* 298 $M^{+\bullet}$, *m/z* 256 $[M\text{-}C_2H_2O]^{+\bullet}$ and intense *m/z* 238 $[M\text{-}CH_3COOH]^{+\bullet}$. In addition, OE ion series from *m/z* 153-55 separated by 14Da and peaks at *m/z* 87 (α-cleavage, $C_4H_7O_2$), 61 ($C_2H_3O_2$) 43 indicating saturated aliphatic chain and acetyl group on position 2. The second peak is heptadec-2-yl-acetate (HDA). HDA have also chiral center at position 2, however 2*R*- and 2*S*-enantiomers were present in 50/50 ratio and only and *rac*-heptadec-2-yl-acetate was prepared and further used in this study.

Third peak with much longer retention (KI 3058) shows in abundant molecular ion *m/z* 448 ($M^{+\bullet}$, accurate mass *m/z* 448.42951 for $C_{30}H_{56}O_2$ calculated 448.428032) and fragment ions at *m/z* 405 $[M\text{-}C_2H_2O]^{+\bullet}$ and *m/z* 388 $[M\text{-}CH_3COOH]^{+\bullet}$ accompanied with EE ion series from *m/z* 264-166 OE series *m/z* 149-67 both spaced by 14Da. Acetate function was deduced from *m/z* 61 ($C_2H_3O_2$) most probably in position 1. Intense ions *m/z* 149, 135, 121 and 109 indicate omega-6 and omega-9 skipped diene structure. Data suggest (*Z,Z*)-19,22-octacosadien-1-yl acetate (OCDA) as the third peak and the proposed structure was confirmed by chemical synthesis.

Chemical synthesis

Commercially available chemicals were used without further purification. Tetrahydrofuran (anhydrous, Sigma-Aldrich) and dichloromethane (Roth) were used as received. All reactions except the enzymatic hydrolysis were carried out under an atmosphere of argon. Preparative column chromatography was performed on Silica gel 60 (230-400 mesh, Carl Roth GmbH) and TLC analysis on commercial Merck silica gel 60 F_{254} plates. NMR spectra were measured on a Bruker Avance 400 NMR spectrometer. Chemical shifts are reported in ppm downfield from TMS.

Synthesis of (*R*) and (*S*,*Z*)-10-Heptadecen-2-ylacetate (R&S-HDEA).

Synthesis of (Z)-10-Heptadecen-2-one.

Palmitoleic acid (250 mg, 0.98 mmol) was dissolved in 10 mL of THF and cooled to -78°C. A 1.6 M solution of MeLi in diethylether (1.53 ml, 2.45 mmol) was added dropwise and the mixture was allowed to warm to room temperature by removing the cooling bath. The reaction was monitored via TLC. Upon completion (after ca. 2.5h) the mixture was poured into 20 mL of 1N HCl at 0°C and extracted with diethylether (3x15 ml). The combined organic layers were washed with saturated $NaHCO_3$ (20 ml) and brine (20 ml), dried with anhydrous $NaSO_4$, filtered and concentrated in vacuo. After purification via silica gel column chromatography (12:1 hexane/EtOAc) (*Z*)-10-Heptadecen-2-one was obtained as colourless oil (225 mg, 91%).^{1}H-NMR: (400 MHz, $CDCl_3$) δ = 5.35 (m, 2H), 2.41 (t, *J* = 7.3 Hz, 2H), 2.13 (s, 3H), 2.01 (q, *J* = 5.7 Hz, 4H), 1.57 (m, 2H), 1.29 (m, 16H), 0.89 (t, *J* = 6.0 Hz, 3H)ppm; ^{13}C-NMR: (100 MHz, $CDCl_3$) δ = 209.2, 130.0, 129.7, 43.8, 31.8, 29.8, 29.72, 29.68, 29.28, 29.15, 29.09, 28.97, 27.22, 27.15, 23.9, 22.6, 14.1 ppm.

Synthesis of (±,Z)-10-Heptadecen-2-yl acetate.

(*Z*)-10-Hexadecen-2-one (100 mg, 0.4 mmol) was dissolved in 20 mL of Ethanol and 15 mg $NaBH_4$ (0.4 mmol) were added. The mixture was stirred at room temperature and after 45 min 5 mL sat. NH_4Cl solution was added. The mixture was extracted with diethylether (3x15 ml). The combined organic layers were washed with water (20 ml) and brine (20 ml), dried with anhydrous $NaSO_4$, filtered and concentrated in vacuo to obtain crude (*Z*)-10-Heptadecen-2-ol. The alcohol was dissolved in 10 mL CH_2Cl_2 and 100 µl Ac_2O, 100 µl NEt_3 and 2 crystals of DMAP were added. The mixture was stirred at room temperature overnight, quenched with 10 ml water and extracted with diethylether (3x15 ml). The combined organic layers were washed with brine (20 mL), dried with anhydrous $NaSO_4$, filtered and concentrated in vacuo. Purification via silica gel column chromatography (12:1 hexane/EtOAc) yielded racemic (*Z)-10*-Heptadecen-2-yl acetate as colourless oil (115 mg, 97%). ^{1}H-NMR: (400 MHz, $CDCl_3$) δ = 5.35 (m, 2H), 4.88 (hex, *J* = 6.3 Hz, 2H), 2.03 (s, 3H), 2.01 (q, *J* = 6.2 Hz, 4H), 1.51 (m, 2H), 1.29 (m, 18H), 1.20 (d, *J* = 6.4 Hz, 3H), 0.89 (t, *J* = 6.8 Hz, 3H) ppm; ^{13}C-NMR: (100 MHz, $CDCl_3$) δ = 170.8, 130.0, 129.8, 71.1, 35.9, 31.8, 29.7, 29.4, 29.2, 29.0, 27.22, 27.15, 25.4, 22.6, 21.4, 19.9, 14.1 ppm; EI-MS [m/z (relative intensity)]: 41 (58), 43 (100), 54 (45), 55 (84), 67 (63), 68 (51), 69 (57), 81 (67), 82 (89), 83 (40), 95 (63), 96 (77), 97 (23), 109 (33), 110 (38), 124 (49), 138 (38), 152 (12), 166 (8), 180 (5), 194 (7), 236 (35), 281 (4 $[M-CH_3]^+$).

Separation of (R)- and (S,Z)-10-Heptadecen-2-yl acetate.

100 mg of (±,*Z*)-10-Heptadecen-2-yl acetate were dissolved in 1 mL of acetone and 7 mL of phosphatebuffer (0,1M, pH = 7.0) were added to create a fine suspension. Immobilized lipase from *Candida antarctica* was added (40 mg, 2,9 U/mg) and the mixture was stirred at room temperature. The reaction was monitored via GC-MS using a chiral column (Cyclodex B, Agilent). After 20 h the mixture was extracted with diethylether (3x10 ml), washed with brine (10 ml), dried with anhydrous $NaSO_4$, filtered and concentrated in vacuo. Purification via silica gel column chromatography (9:1 hexane/EtOAc) yielded pure (*R,Z*)-10-Heptadecen-2-ol (27 mg) and (*Z*)-10-Heptadecen-2-yl acetate (67 mg of a 3:1 mixture of the (*S*)- and (*R*)-enantiomer). (*R,Z*)-10-Heptadecen-2-ol was reacetylated using the same protocol as described before to give (*R,Z*)-10-Heptadecen-2-yl acetate (25mg, ee = 99%, optical rotation: $[\alpha]^{20}_{589}$ = +1.3, 3.01 mg/mL hexane). The remaining mixture of the (*S*) and (*R*)-enantiomer was again subjected to enzymatic hydrolysis until all of the remaining (*R*)-enantiomer was hydrolysed (ca. 48h). The mixture was worked up as described before and purified via silica gel column chromatography (9:1 hexane/EtOAc) to obtain (*S,Z*)-10-Heptadecen-2-yl acetate (31 mg, ee = 97.5%, optical rotation: $[\alpha]^{20}_{589}$ = -1.4, 3.55 mg/mL hexane).

Synthesis of Heptadec-2-yl acetate (HDA)

Synthesis of Heptadecan-2-one.

Palmitic acid (1.6 g, 6.25 mmol) was dissolved in 25 mL of THF and cooled to -78°C. A 1.6 M solution of MeLi in diethylether (8.6 ml, 13.75 mmol) was added dropwise and the mixture was allowed to warm to room temperature by removing the cooling bath. The reaction was monitored via TLC. Upon completion (after ca. 2.5h) the mixture was poured into 40 mL of 1N HCl at 0°C and extracted with diethylether (3x40 ml). The combined organic layers were washed with saturated $NaHCO_3$ (50 ml) and brine (50 ml), dried with anhydrous $NaSO_4$, filtered and concentrated in vacuo. After purification via silica gel column chromatography (12:1 hexane/EtOAc) Heptadecan-2-one was obtained as white wax (1.4 g, 90%). ^{1}H-NMR: (400 MHz, $CDCl_3$) δ = 2.41 (t, *J* = 7.5 Hz, 2H), 2.13 (s, 3H), 1.57 (m, 2H), 1.29 (m, 26H), 0.89 (t, *J* = 6.8 Hz, 3H) ppm; ^{13}C-NMR: (100 MHz, $CDCl_3$) δ = 209.4, 43.8, 31.9, 29.8, 29.7, 29.7, 29.6, 29.5, 29.4, 29.3, 29.2, 23.9, 22.7, 14.1 ppm.

Synthesis of (±)-Heptadecan-2-ol.

Heptadecan-2-one (1.35 g, 5.3 mmol) was dissolved in 100 mL of ethanol and $NaBH_4$ (0.8 g, 21 mmol) was added at 0°C. The mixture was stirred for 2h at room temperature, quenched with 50 mL of sat. NH_4Cl-solution diluted with 50 mL water and extracted with diethylether (2x100 ml). The combined organic layers were washed with saturated $NaHCO_3$ (50 ml) and brine (50 ml), dried with anhydrous $NaSO_4$, filtered and concentrated in vacuo. The residue was chromatographed on silica gel (9:1 hexane/EtOAc) to yield (±)-Heptadecan-2-ol as a white wax (1.2 g, 88%). ^{1}H-NMR: (400 MHz, $CDCl_3$) δ = 3.78 (h, *J* = 5.9 Hz, 1H), 1.20-1.52 (m, 28H), 1.18 (t, *J* = 5.9 Hz, 3H), 0.88 (d, *J* = 6.6 Hz, 3H)ppm; ^{13}C-

NMR: (100 MHz, $CDCl_3$) δ = 68.2, 39.4, 31.9, 29.67, 29.64, 29.61, 29.60, 29.3, 25.8, 23.5, 22.7, 14.1 ppm.

Synthesis of (±)-Heptadec-2-yl acetate.

(±)-Heptadecan-2-ol (1.17 g, 4.6 mmol) was dissolved in 20 mL CH_2Cl_2 and 940 μL Ac_2O, 1.4 mL NEt_3 and 20 mg of DMAP were added. The mixture was stirred at room temperature for 3h, quenched with 20 mL ice-water and extracted with diethylether (3x30 ml). The combined organic layers were washed with water (40 ml) and brine (40 ml), dried with anhydrous $NaSO_4$, filtered and concentrated in vacuo. Purification via silica gel column chromatography (12:1 hexane/EtOAc) yielded (±)-Heptadec-2-yl acetate as a white wax (1.36 g, 99%). ^{1}H-NMR: (400 MHz, $CDCl_3$) δ = 4.88 (h, *J* = 6.3 Hz, 1H), 2.02 (s, 3H), 1.51 (m, 2H), 1.20-1.37 (m, 26H), 1.20 (d, *J* = 6.3 Hz, 3H), 0.88 (t, *J* = 6.8 Hz, 3H)ppm; ^{13}C-NMR: (100 MHz, $CDCl_3$) δ = 170.5, 71.1, 35.9, 31.9, 29.68, 29.65, 29.61, 29.57, 29.53, 29.45, 29.35, 25.4, 22.7, 21.4, 19.9, 14.1 ppm; EI-MS data in agreement with data from Wiley Subscription Services, Inc. (US) via SciFinder.

Synthesis of (19*Z*,22*Z*)- Octacosadienyl acetate (OCDA).

Synthesis of 3-Eicosyn-1-ol.

Freshly prepared THP-protected 3-Butynol (*61*) (2.5 g, 16.23 mmol) was added dropwise to a suspension of $NaNH_2$ (1.54 g of a 50% suspension in toluene, 19.5 mmol) in THF (15 ml) at 0°C. After 1h, DMSO (15 ml) and 1-Bromohexadecane (5.4 g, 17.7mmol) were added and the mixture was stirred for 3h at room temperature. The reaction mixture was quenched with water (20 ml) and extracted with diethylether (3 × 25 ml). The combined organic phases were washed with brine and dried over $MgSO_4$. After filtration, the solvent was removed via rotavap and the residue was chromatographed on silica gel (20:1 to 15:1 hexane/EtOAc) to obtain 1-[Tetrahydropyranyl)oxy]-3-eicosyne, which was immediately dissolved in 30 mL MeOH and treated with 20 mg *p*-Toluenesulfonic acid. After 1h at room temperature, 20 mL of saturated $NaHCO_3$-solution were added and the mixture was extracted with diethylether (3 × 25ml). The combined organic phases were washed with water (25 ml) and brine (15 ml) and dried over $MgSO_4$. After filtration, the solvent was removed via rotavap and the residue was chromatographed on silica gel (9:1 hexane/EtOAc) to obtain 3-Eicosyn-1-ol (2.1 g, 44% yield over two steps). ^{1}H-NMR: (400 MHz, $CDCl_3$) δ = 3.67 (t, *J* = 6.3 Hz, 2H), 2.41 (tt, ^3J = 9.3 Hz, ^5J = 2.4 Hz, 2H), 2.14 (tt, ^3J = 10.6 Hz, ^5J = 2.4 Hz, 2H), 1.48 (m, 2H), 1.30 (m, 26H), 0.89 (t, *J* = 6.8 Hz, 3H)ppm; ^{13}C-NMR: (100 MHz, $CDCl_3$) δ = 82.5, 76.3, 61.3, 31.9, 29.7, 29.6, 29.5, 29.4, 29.3, 29.2, 29.1, 29.0, 28.9, 23.1, 22.6, 18.7, 14.0 ppm.

Synthesis of 19-Eicosyn-1-ol.

Ethylene-1,2-diamine (11 ml) was cooled to 0°C and 1.02 g NaH (60% in mineral oil, 25.5 mmol) were added. The mixture was allowed to warm to room temperature and stirred for 2 h. The violet mixture was heated to 60°C and stirred for 1h, before it was cooled to 40°C. At this temperature 3-eicosyn-1-ol (1.2 g, 4 mmol) was added. The green reaction mixture was then heated to 70°C and stirred for 5 h. After cooling to 0°C HCl_{aq} (0.5 M, 20 ml) was added very carefully. The mixture was poured into a separatory funnel and HCl_{aq} (1 M, 20ml) was added before extracting with diethylether (3 × 20 ml). The combined organic phases were washed with HCl_{aq} (1 M, 30ml) and brine (30 ml), dried over Na_2SO_4 and concentrated under vacuum. Purification was done via column chromatography on silica gel (9:1 *n*-hexane/EtOAc) and 19-Eicosyn-1-ol (780 mg, 65%) was obtained as a white waxy solid. ^{1}H-NMR: (400 MHz, $CDCl_3$) δ = 3.64 (t, *J* = 6.6 Hz, 2H), 2.17 (td, ^3J = 10.3 Hz, ^4J = 2.6 Hz, 2H), 1.94 (t, *J* = 2.7 Hz, 1H), 1.54 (m, 4H), 1.30 (m, 28H) ppm; ^{13}C-NMR: (100 MHz, $CDCl_3$) δ = 84.8, 68.0, 63.1, 32.8, 29.7, 29.6, 29.5, 29.4, 29.3, 29.1, 28.8, 28.5, 25.7, 18.4 ppm.

Synthesis of 19,22-Octacosadiyn-1-ol.

To a suspension of CuI (1.01g, 5.3 mmol), NaI (800 mg, 5.3 mmol) and K_2CO_3 (554 mg, 4 mmol) in DMF (10 ml), 1-bromo-2-octyn (550 mg, 2.91 mmol) and 19-Eicosyn-1-ol (780 mg, 2.65 mmol) were added. The suspension was stirred overnight and filtered over Celite®. The filtrate was poured into 20 mL of sat. NH_4Cl and extracted with diethylether (3 × 30 ml). The combined organic phases were washed with brine (30 ml), dried over Na_2SO_4 and concentrated under vacuum. Purification was done via column chromatography on silica gel (12:1 *n*-hexane/EtOAc) and *19*,*22*-Octacosadiyn-1-ol (737 mg,

69%) was obtained as a white waxy solid. ^{1}H-NMR: (400 MHz, $CDCl_3$) δ = 3.63 (t, *J* = 6.5 Hz, 2H), 3.12 (quin, ^{5}J = 2.4 Hz, 2H), 2.14 (tt, ^{3}J = 10.5 Hz, ^{5}J = 2.3 Hz, 4H), 1.52 (m, 6H), 1.30 (m, 32H), 0.90 (t, *J* = 6.4 Hz, 3H) ppm; ^{13}C-NMR: (100 MHz, $CDCl_3$) δ = 80.5, 74.5, 63.0, 32.8, 31.1, 29.7, 29.6, 29.5, 29.4, 29.3, 29.1, 29.0, 28.9, 28.8, 28.5, 25.7, 22.2, 18.72, 18.70, 13.9, 9.7 ppm.

Synthesis of 19,22-Octacosadiynyl acetate.

19,22-Octacosadiyn-1-ol (435 mg, 1.08 mol) were dissolved in 10 mL dichloromethane. Acetic anhydride (234 μL, 2.2 mmol), triethylamine (345 μL, 2.2 mmol) and a few crystals of 4-dimethylaminopyridine were added and the solution stirred for 2 h. Water (10 ml) was added and the mixture was extracted with diethylether (3 × 15 ml). The combined organic phases were washed with brine (30 ml), dried over Na_2SO_4 and concentrated under vacuum. Purification was done via column chromatography on silica gel (25:1 *n*-hexane/EtOAc) and 19,22-Octacosadiynyl acetate (435 mg, 90%) was obtained as a white waxy solid. ^{1}H-NMR: (400 MHz, $CDCl_3$) δ = 4.05 (t, *J* = 6.8 Hz, 2H), 3.11 (quin, ^{5}J = 2.4 Hz, 2H), 2.14 (tt, ^{3}J = 10.7 Hz, ^{5}J = 2.3 Hz, 4H), 2.04 (s, 3H), 1.61 (quin, *J* = 7.0 Hz, 2H), 1.48 (m, 4H), 1.30 (m, 32H), 0.89 (t, *J* = 6.7 Hz, 3H) ppm; ^{13}C-NMR: (100 MHz, $CDCl_3$) δ = 171.2, 80.4, 74.5, 64.6, 31.1, 29.7, 29.6, 29.5, 29.4, 29.3, 29.1, 28.9, 28.8, 28.6, 28.5, 25.9, 22.2, 21.0, 18.72, 18.70, 13.9, 9.7 ppm.

Synthesis of (19Z,22Z)-Octacosadienyl acetate.

19,22-Octacosadiyn-1-ol acetate (200 mg, 0.44 mmol) was dissolved in 4 mL MeOH and hydrogenated in an H_2-atmosphere in the presence of 15 mg Lindlar catalyst (Sigma). The reaction was monitored via GC-MS and after completion (ca. 15 h) the mixture was diluted with diethylether (15 ml), filtered over Celite® and concentrated in vacuum. Purification was done via reversed-phase column chromatography on C18-silica gel (3:1 MeOH/$CHCl_3$) to obtain 19*Z*,22*Z*-Octacosadienyl acetate (180 mg, 91%) as a white waxy solid. ^{1}H-NMR: (400 MHz, $CDCl_3$) δ = 5.35 (m, 4H), 4.05 (t, *J* = 6.8 Hz, 2H), 2.77 (t, *J* = 6.4 Hz, 2H), 2.05 (q, *J* = 6.8 Hz, 4H), 2.04 (s, 3H), 1.61 (quin, *J* = 7.0 Hz, 2H), 1.30 (m, 32H), 0.89 (t, *J* = 6.8 Hz, 3H) ppm; ^{13}C-NMR: (100 MHz, $CDCl_3$) δ = 171.2, 130.2, 128.0, 64.7, 31.5, 29.7, 29.6, 29.5, 29.4, 29.3, 29.2, 28.6, 27.25, 27.20, 25.9, 25.6, 22.6, 21.0, 14.1 ppm; EI-MS [m/z (relative intensity)]: 54 (25), 55 (100), 56 (22), 57 (41), 61 (22), 67 (50), 68 (41), 69 (78), 70 (17), 71 (18), 80 (13), 81 (53), 82 (80), 83 (71), 84 (10), 85 (10), 95 (50), 96 (78), 97 (52), 109 (31), 110 (34), 111 (22), 123 (20), 124 (21), 137 (13), 138 (14), 152 (12), 390 (37), 391 (11), 448 (17 $[M]^+$).